Alma Mater Studiorum - Università di Bologna
in cotutela con l'Università di Strasburgo

Tesi di
Dottorato di ricerca in Fisica
Ciclo XXVII

Settore concorsuale di afferenza: 02/A2
Settore Scientifico Disciplinare: FIS/02

Correlations and Quantum Dynamics of 1D Fermionic Models: New Results for the Kitaev Chain with Long-Range Pairing

presentata da Davide Vodola

Coordinatore Dottorato:
prof. Fabio Ortolani

Relatore:
prof.ssa Elisa Ercolessi

Relatore:
prof. Guido Pupillo

Esame finale anno 2015

Abstract

In the first part of the thesis, we propose and analyze an exactly-solvable one-dimensional model for fermions with long-range p-wave pairing decaying with distance ℓ as a power law $1/\ell^{\alpha}$. We studied the phase diagram by analyzing the critical lines, the decay of correlation functions and the scaling of the von Neumann entropy with the system size. We found two types of gapped regimes, where correlation functions decay (i) exponentially at short distance and algebraically at long distance ($\alpha > 1$), or (ii) purely algebraically ($\alpha < 1$). In the latter a violation of the area law (i.e. a logarithmic scaling) for the entanglement entropy is also observed. Most interestingly, along the critical lines, long-range pairing is found to break the conformal symmetry of the model for sufficiently small α. This can be detected also via the dynamics of entanglement following a quench.

In the second part of the thesis we studied the evolution in time of the entanglement entropy when the system is driven across a quantum phase transition with different velocities. We analyzed the Ising model in a transverse field varying linearly in time with different velocities. We computed the time-evolution of the entanglement entropy of half chain and we found that it displays different regimes depending on the velocity at which the critical point is reached: an adiabatic one (small velocities) when the system evolves according the instantaneous ground state; a sudden quench (large velocities) when the system is essentially frozen to its initial state; and an intermediate one, where the entropy starts growing linearly but then displays oscillations (also as a function of the velocity). Finally, we discussed the Kibble-Zurek mechanism for the transition between the paramagnetic and the ordered phase.

Contents

Introduction

Recent experimental progress in trapping and manipulating cold and ultra-cold atomic and molecular gases [1–3] has offered the possibility to explore and simulate a wide class of phenomena occurring in many-body systems both at and out of the equilibrium. Examples includes the observations of strongly correlated phases and quantum phase transitions [4–10] and of out-of-equilibrium phenomena such as (quasi-)particle transport and dynamical propagation of correlations [11–19].

Optical lattices [20] are the key example of structures in which the atoms can be trapped in a well-controlled way offering the possibility to modify geometry, lattice spacing and kinetic energy with extreme versatility while interactions among them can be changed in strength with Feshbach resonances [21], using external fields.

It has become now possible to tune for the first time also the range and the shape of the interactions, for example, by using Rydberg atoms [22–25] and, very recently, trapped ions [19, 26–28]. They have been successfully employed for creating potentials decaying with distance r as $1/r^{\alpha}$ where α can be tuned between 0 and 3.

It is, however, an open question to understand the properties analytically of systems with long-range interactions.

In the first part of this thesis we investigate an exactly solvable model for fermions with a long range pairing, in particular we clarify the structure of the static phase diagram and behavior of nonlocal quantities (such as the correlation functions and the entanglement entropy).

The Hamiltonian H we analyzed, given by

$$\begin{aligned} H = &-w \sum_{j} \left(a_j^{\dagger} a_{j+1} + \text{h.c.} \right) - \mu \sum_{j} \left(n_j - \frac{1}{2} \right) \\ &+ \frac{\Delta}{2} \sum_{j,\ell} \frac{1}{\ell^{\alpha}} \left(a_j a_{j+\ell} + a_{j+\ell}^{\dagger} a_j^{\dagger} \right), \end{aligned} \tag{1}$$

is a generalization of the Kitaev chain [29] describing a fermionic system with long-range p-wave pairing, decaying with distance ℓ as $1/\ell^{\alpha}$.

The original Kitaev Hamiltonian with only on-site or nearest-neighboring terms, has been studied as a model for topologically ordered phase in one dimension. A topological one-dimensional phase is characterized

by two or more degenerate low-energy lying states appearing without the breaking of any local order parameter.

As the system is in a gapped phase, these states also remain well separated from the rest of the spectrum and, in the case of an open chain, two modes are found to be localized at the edges of the system. They have been identified with two Majorana fermions and they have attracted much interest for quantum computing because they can be employed, in principle, as qubits, being robust against decoherence.

The long-range model we analyzed remains still quadratic in terms of the fermionic operators and, thus, it is still exactly solvable. Using the integrability of the model, we were able to compute exactly the decay of the correlation functions, a task not always achievable for a general Hamiltonian and to demonstrate the existence of two types of gapped regimes, where correlation functions decay exponentially at short range and algebraically at long range ($\alpha > 1$) or purely algebraically ($\alpha < 1$).

In the same gapped regions where the correlators decay as a power law, the entanglement entropy of a subsystem if found to diverge logarithmically. Both these results are unexpected in massive phases of local Hamiltonians where correlation functions decay purely exponentially [30] and entanglement entropy saturates to a constant [31], in fact these effects are very peculiar to systems with strong long-range interactions.

If one considers the limit $\alpha \to \infty$ the model reduces, after a Jordan-Wigner transformation, to the XY-Ising model with pure nearest-neighbor interactions [32–34]. The latter has been widely studied because it is exactly solvable and, at the same time, it is able to explain non trivial phenomena.

The XY model can be considered as a paradigm for the quantum phase transition [35] between a paramagnetic and an ordered phase separated by a critical point and it defines an universality class for the phase transition described by a conformal gapless field theory [36, 37].

In our work, we find that by introducing the long-range term in the Hamiltonian, this point, for sufficiently small α, is no more described by a conformal field theory. This can be also proven by computing the time evolution of the entanglement entropy following a quench.

In a conformal invariant model, it was shown that the entropy grows linearly in time [38]. This can be understood if one thinks that, following a quench, in a given point of the system, quasiparticles excitations are created. These excitations are carried by couples of entangled particles moving with opposite momenta and opposite finite group velocities. If now one cuts the system into two parts (say A and B), the rate of arrival in B of quasiparticles created in A is constant (because group velocities are constant) and the growth of entanglement between the two regions is linear in time.

We find that the time evolution of the entropy in the chain with the long-range pairing, instead, shows a logarithmic growth when $\alpha \lesssim 1$. The same has been observed for the Ising model with long range interactions [39] and

it is related to the appearance of a divergent quasi-particle velocity. For our model, we found, indeed, the exact point in the phase diagram where the divergence of the quasiparticle velocity appears.

More related to the problem of the dynamics in closed quantum systems, the second part of the thesis deals with the time evolution of the entanglement entropy and the entanglement spectrum when the system is driven across a quantum phase transition with different speeds.

As key example, we focus on the transverse-field Ising model with a time-dependent magnetic field varying linearly in time:

$$H_{\text{Ising}} = \sum \left[\sigma_i^x \sigma_{i+1}^x - h(t)\sigma_i^z\right] \tag{2}$$

where σ_i^x and σ_i^z are Pauli matrices. The magnetic field varies as $h(t) = h_i + \frac{t}{\tau}$, where τ is the inverse of the velocity at which the system is driven and we choose $h_i > 1$ to in the paramagnetic phase.

We computed the time-evolution of the entanglement entropy of half chain and we found that it displays different regimes depending on the speed at which the critical point is reached: an adiabatic one (small velocities, large τ) when the system evolves according the instantaneous ground state; a sudden quench (large velocities, small τ) when the system is essentially frozen to its initial state; and an intermediate one, where the entropy starts growing linearly (because of the quasiparticle picture discussed before) but then displays oscillations in time (also as a function of the velocity) because the system ends up, after passing the critical point, in a superposition of excited states of the instantaneous Hamiltonian.

We also discussed the Kibble-Zurek mechanism [40–43] for the transition between the paramagnetic and the ordered phase. Kibble-Zurek mechanism predicts the scaling of the number of topological defects produced after the dynamical transition of a critical point driven by the temperature (or also by an external field in the case of a quantum phase transition at zero temperature).

The evolution of the system can be divided into three parts: a first one, where the system will respond adiabatically to the change of the external field. A second impulsive, in the vicinity of the critical point where the correlation length ξ starts to diverge and the adiabatic behavior is obliviously violated. Here we have also the formation of topological defects on distances smaller than ξ that scales, according Kibble-Zurek mechanism, as $\xi \sim \tau^{\nu/(\nu z+1)}$ where τ is the inverse of the velocity with which the critical point is reached and ν and z are the critical exponent of the transition.

As the entropy S, in a gapped region, is found to be proportional to the logarithm of the correlation length ξ ($S \sim \log \xi$ [31]), we showed the entropy to scale, because of Kibble-Zurek argument, as $S \sim \log \tau$.

The thesis is organized as follows: in Chapter 1, we introduce the Hamiltonian of the Kitaev chain with long range pairing and then discuss its ex-

act solution (Sec. 1.1), the critical lines (Sec. 1.2), the decay of the correlation functions (Sec. 1.3), the scaling of the von Neumann entropy both with the system size (Sec. 1.4) and in time after a quench (Sec. 1.5) and finally, for an open chain, the emergence of the edge modes (Sec. 1.6).

Appendices contain some exact computations for the finite size corrections to the ground state energy density of the Ising model (Appendix 1.A), details on the technique for computing the entanglement spectrum of quadratic models (Appendix 1.B), and the definition with some basic properties of polylogarithms (Appendix 1.C).

In Chapter 2, we analyze the scaling in time of the entanglement entropy for the Ising model with a time-dependent magnetic field. We describe the adiabatic and the sudden regimes (Sec. 2.2.1), the fast (Sec. 2.2.2) and the slow (Sec. 2.2.3) sweeps and, finally, the Kibble-Zurek physics (Sec. 2.3). Appendix 2.A contains the computation of the initial density matrix.

The results from the first and second part of this thesis have been collected in two papers and have been published during the PhD.

The first part can be found in

D. Vodola, L. Lepori, E. Ercolessi, A. V. Gorshkov, G. Pupillo,
Kitaev chains with long-range pairing,
Phys. Rev. Lett. **113**, 156402 (2014)

while the second in

E. Canovi, E. Ercolessi, P. Naldesi, L. Taddia, D. Vodola,
Dynamics of entanglement entropy and entanglement spectrum crossing a quantum phase transition,
Phys. Rev. B **89**, 104303 (2014).

1
Kitaev chain with long-range pairing

One of the most important exact solvable model for spins interacting in a one dimensional chain is the quantum Ising model. This model describes the quantum phase transition between a disordered paramagnetic and an ordered phase driven by an external magnetic field h.

In the model Hamiltonian

$$H_{\text{Ising}} = \sum_i \left[\sigma_i^x \sigma_{i+1}^x - h\sigma_i^z\right] \tag{1.1}$$

the interaction term describes the coupling between two neighboring $1/2$ spins ($\sigma_i^{(x,z)}$ are Pauli matrices) and is minimized if two spins are anti-aligned along the x direction (ordered phase). The magnetic field, instead, tries to align them along the z direction, so there should be a critical value h_c of the magnetic field for which the order in the x direction is destroyed (paramagnetic or disordered phase). In Appendix 1.A, I will review the exact solution of this model.

It was found that this Hamiltonian is equivalent to a free-fermionic model. By means of the Jordan-Wigner transformation [44]

$$\sigma_i^+ = \frac{1}{2}\left(\sigma_i^x + \mathrm{i}\sigma_i^y\right) = a_i^\dagger \mathrm{e}^{\mathrm{i}\pi \sum_{l=1}^{i-1} a_l^\dagger a_l} \tag{1.2}$$

$$\sigma_i^- = \frac{1}{2}\left(\sigma_i^x - \mathrm{i}\sigma_i^y\right) = a_i \mathrm{e}^{-\mathrm{i}\pi \sum_{l=1}^{i-1} a_l^\dagger a_l} \tag{1.3}$$

$$\sigma_i^z = 2a_i^\dagger a_i - 1 \tag{1.4}$$

one can write spin $1/2$ operators in terms of fermionic operators and thus cast (1.1) in this form

$$H_{\text{Ising}} = \sum_j \left(a_j^\dagger a_{j+1} + a_j^\dagger a_{j+1}^\dagger + \text{h.c.}\right) - h\sum_j \left(2a_j^\dagger a_j - 1\right). \tag{1.5}$$

From its first appearance, this transformation has been considered only as a mathematical technique both to map spin into fermionic degrees of freedom and to simplify computation of physical quantities of (1.1) and similar models. Now, as fermions can be trapped in one dimensional systems (e.g. in quantum wires), the model (1.5) can describe the actual dynamics of fermionic particles in a lattice.

The first interpretation of the different phases of the Ising model in term of fermionic language was given by Kitaev in [29]. He found that the spin ordered phase corresponds to a topological order, meaning that the Hamiltonian has two degenerate (in the thermodynamic limit) ground states, separated by a finite gap from the remaing spectrum and, the order parameter, local in terms of spin operators, is non-local if written in terms of fermionic operators.

In this Chapter we will introduce and analyze a generalization of the Kitaev chain for fermions with long-range pairing, which decays with distance as a power-law.

1.1 The model

We considered the following Hamiltonian for fermionic particles on a lattice of L sites:

$$\begin{aligned} H = &-w \sum_j \left(a_j^\dagger a_{j+1} + \text{h.c.} \right) - \mu \sum_j \left(n_j - \frac{1}{2} \right) \\ &+ \frac{\Delta}{2} \sum_{j,\ell} d_\ell^{-\alpha} \left(a_j a_{j+\ell} + a_{j+\ell}^\dagger a_j^\dagger \right). \end{aligned} \tag{1.6}$$

Here, $a_j^\dagger$ (a_j) is a fermionic creation (annihilation) operator on site j, $n_j = a_j^\dagger a_j$, and w is the tunneling rate on a lattice with unit lattice constant. The quantities μ and Δ are the chemical potential and the strength of the fermion p-wave pairing, respectively.

The decay of the pairing term is given by the function d_ℓ specifying the distance between two fermions. If the lattice is a closed ring, the maximum distance will be $L/2$ and $d_\ell = \min(\ell, L - \ell)$, while if the lattice is a closed linear chain $d_\ell = \ell$. In both the cases the pairing decays with distance ℓ as a power law with exponent α.

Hamiltonian (1.6), even with the long-range pairing, is still exactly solvable. So, we were able to determine the phase diagram (Fig. 1.5) by diagonalizing it exactly and to analyze (i) the critical points; (ii) the decay of the correlation functions; (iii) the scaling of the entanglement entropy with the system size in detail.

1.1.1 Exact diagonalization

Let us consider the case of a closed translationally invariant ring ($d_\ell = \min(\ell, L - \ell)$). The choice of the boundary conditions for the fermions is dictated by the pairing term.

The terms $a_j a_{j+\ell}$ and $a_{j+\ell} a_{j+\ell+L}$ in the pairing connect two fermions with the same distance ℓ because of the ring geometry.

If we consider periodic boundary conditions ($a_i = a_{i+L}$) the two terms will sum up to zero because of the anti-commutation relations for the fermions and the pairing term will cancel out. For this reason, we need anti-periodic boundary conditions ($a_i = -a_{i+L}$).

This choice, anyway, does not affect the final results because, as we will do, one can consider an infinite-long system.

The translationally invariance of the ring lets us to use a Fourier transform for the fermionic operators $a_i^\dagger = \frac{1}{\sqrt{L}} \sum_{n=0}^{L-1} e^{ik_n x_i} \tilde{a}_{k_n}^\dagger$ and, because of anti-periodic boundary conditions, lattice momenta will be quantized as $k_n = \frac{2\pi}{L}\left(n + \frac{1}{2}\right)$.

In this basis, Hamiltonian (1.6) reads:

$$\begin{aligned} H = &- \sum_n \left(w \cos k_n + \frac{\mu}{2}\right)\left(\tilde{a}_{k_n}^\dagger \tilde{a}_{k_n} + \tilde{a}_{-k_n}^\dagger \tilde{a}_{-k_n}\right) \\ &+ i\frac{\Delta}{2} \sum_n f_\alpha(k_n)\left(\tilde{a}_{k_n}\tilde{a}_{-k_n} - \tilde{a}_{-k_n}^\dagger \tilde{a}_k^\dagger\right) + \frac{\mu L}{2} \end{aligned} \tag{1.7}$$

with

$$f_\alpha(k) = \sum_{\ell=1}^{L-1} \frac{\sin(k\ell)}{d_\ell^\alpha} \tag{1.8}$$

the function containing the information on the long-range pairing (see Appendix 1.C).

This Hamiltonian is in block-diagonal form, each of the block corresponding to a different momentum k_n:

$$H = \frac{1}{2} \sum_{n=0}^{L-1} \begin{pmatrix} \tilde{a}_{k_n}^\dagger & \tilde{a}_{-k_n} \end{pmatrix} \begin{pmatrix} -(2w\cos k_n + \mu) & i\Delta f_\alpha(k_n) \\ -i\Delta f_\alpha(k_n) & (2w\cos k_n + \mu) \end{pmatrix} \begin{pmatrix} \tilde{a}_{k_n} \\ \tilde{a}_{-k_n}^\dagger \end{pmatrix} \tag{1.9}$$

We can diagonalize H in each of the blocks by a Bogolyubov transformation:

$$\begin{pmatrix} a_{k_n} \\ a_{-k_n}^\dagger \end{pmatrix} = \mathbb{U}^\dagger \begin{pmatrix} \eta_{k_n} \\ \eta_{-k_n}^\dagger \end{pmatrix} \tag{1.10}$$

with

$$\mathbb{U} = \begin{pmatrix} \cos\theta_{k_n} & i\sin\theta_{k_n} \\ i\sin\theta_{k_n} & \cos\theta_{k_n} \end{pmatrix} \tag{1.11}$$

and θ_{k_n} given by

$$\tan(2\theta_{k_n}) = -\frac{\Delta f_\alpha(k_n)}{2w\cos k_n + \mu} \tag{1.12}$$

The Hamiltonian in the Bogolyubov basis becomes:

$$H = \sum_{n=0}^{L-1} \lambda_\alpha(k_n)\left(\eta_{k_n}^\dagger \eta_{k_n} - \frac{1}{2}\right) \tag{1.13}$$

each fermion η_{k_n} carrying an energy

$$\lambda_\alpha(k_n) = \sqrt{\left(2w\cos k_n + \mu\right)^2 + \left(\Delta f_\alpha(k_n)\right)^2} \tag{1.14}$$

As the Hamiltonian does not commute with the total number of a_{k_n} fermions, the ground state is the vacuum of the Bogolyubov η_{k_n} fermions and it has a BCS-like structure:

$$|\mathrm{GS}\rangle = \prod_{n=0}^{L/2-1} \left(\cos\theta_{k_n} - \mathrm{i}\sin\theta_{k_n}\tilde{a}^\dagger_{k_n}\tilde{a}^\dagger_{-k_n}\right)|0\rangle \tag{1.15}$$

where $|0\rangle$ is the vacuum of a_{k_n} and its energy density is

$$e_\alpha(L) = -\frac{1}{2L}\sum_{n=0}^{L-1}\lambda_\alpha(k_n). \tag{1.16}$$

1.2 Critical lines

To find the critical lines of the Hamiltonian, we consider the thermodynamic limit $L \to \infty$, so momenta will belong to the continuous interval $k \in [0, 2\pi)$ and the dispersion relation will be

$$\lambda^\infty_\alpha(k) = \sqrt{\left(2w\cos k + \mu\right)^2 + \left(\Delta f^\infty_\alpha(k)\right)^2} \tag{1.17}$$

with $f^\infty_\alpha(k) = -\mathrm{i}(\mathrm{Li}_\alpha(\mathrm{e}^{\mathrm{i}k}) - \mathrm{Li}_\alpha(\mathrm{e}^{-\mathrm{i}k}))$ and $\mathrm{Li}_\alpha(x)$ the polylogarithm functions (Appendix 1.C).

Critical lines can be determined by studying $f^\infty_\alpha(k)$. As we discuss in Appendix 1.C, when $\alpha > 1$, $f^\infty_\alpha(k_c) = 0$ for $k_c = 0$ or $k_c = \pi$, so both the lines $\mu = 2w$ and $\mu = -2w$ are critical. When $\alpha \leq 1$ $f^\infty_\alpha(k_c) = 0$ only for $k_c = \pi$ so, the line $\mu = 2w$ is still critical, while the line $\mu = -2w$ is gapped because $f^\infty_\alpha(k) \to \infty$ if $k \to 0$.

In this way it is now possible to connect the disordered phase $|\mu| > 2w$ in the limit $\alpha \to \infty$ with the ordered one $|\mu| < 2w$ without closing the gap.

Let us consider the limit $\alpha \to \infty$. If we use the Jordan Wigner transformation and we express the fermionic operators in terms of spin 1/2 matrices we get the Hamiltonian of the XY model (Appendix 1.A):

$$H(\alpha \to \infty) = -\frac{1}{2}\sum_j \left((w+\Delta)\sigma^x_j\sigma^x_{j+1} + (w-\Delta)\sigma^y_j\sigma^y_{j+1}\right) - \frac{\mu}{2}\sum_j \sigma^z_j. \tag{1.18}$$

At criticality, when $\mu = \pm 2w$, this Hamiltonian is equivalent to that of a free massless fermionic particle and it is described by a conformal field theory [36, 37, 45].

The conformal symmetry of the model, corresponding to the symmetry for translations, rotations and dilations, fixes, among the others, the finite size scaling of the ground-state energy density in a universal way:

$$e(L) = e^{\infty} - \frac{\pi v_F c}{6L^2} \tag{1.19}$$

where both e^{∞}, the energy density in the thermodynamic limit and v_F the Fermi velocity are model-dependent. The previous expression can be used to read the central charge c that can be understood as the number of fermionic massless degrees of freedom in the theory, each fermion counting for $1/2$.

If we compute (1.19) for the XY model (Appendix 1.A) we get

$$e_{XY}(L) = e^{\infty}_{XY} - \frac{\pi v_F}{12L^2} \tag{1.20}$$

and the central charge is $c = 1/2$, as expected.

For the model with long-range pairing one can also compute the finite-size corrections (eq. (1.157)) to the ground-state energy density (1.16) in the same way

$$e_{\alpha}(L) = e_{\infty}(\alpha) + \frac{\pi}{12L^2}\left[\lambda^{\infty}_{\alpha}{}'(\pi) - \lambda^{\infty}_{\alpha}{}'(0)\right] \tag{1.21}$$

with $e_{\infty}(\alpha) = -\int_0^{\pi} \lambda^{\infty}_{\alpha}(x)\mathrm{d}x$ being the energy density in the thermodynamical limit.

The two contributions from $k = 0$ and $k = \pi$ give the corrections to the ground-state energy. We compute them in the following section.

Divergence of the quasi-particle velocity

Let us consider the line $\mu = 2w$, where we study the behavior of $\lambda^{\infty}_{\alpha}(k)$ and of the quasi-particle velocity

$$\frac{\mathrm{d}\lambda^{\infty}_{\alpha}(k)}{\mathrm{d}k} = \frac{1}{\lambda^{\infty}_{\alpha}(k)}\left(-4t^2 \sin k(\cos k + 1) + \Delta^2 f^{\infty}_{\alpha}(k)\frac{\mathrm{d}f^{\infty}_{\alpha}(k)}{\mathrm{d}k}\right), \tag{1.22}$$

both for $k \to 0$ and $k \to \pi$.

We start from the expansion of the polylogarithm [46]

$$\mathrm{Li}_{\alpha}(\mathrm{e}^{\mathrm{i}k}) = \Gamma(1-\alpha)(-\mathrm{i}k)^{\alpha-1} + \sum_{n=0}^{\infty}\frac{\zeta(\alpha-n)}{n!}(\mathrm{i}k)^n \tag{1.23}$$

giving

$$f^{\infty}_{\alpha}(k) = 2\cos\frac{\pi\alpha}{2}\Gamma(1-\alpha)k^{\alpha-1} + 2\sum_{n=1}^{\infty}\sin\frac{\pi n}{2}\frac{\zeta(\alpha-n)}{n!}k^n \tag{1.24}$$

and

$$\begin{aligned} f_\alpha^\infty(k)^2 &= 4\cos^2\frac{\pi\alpha}{2}\Gamma^2(1-\alpha)k^{2\alpha-2} \\ &+ 8\cos\frac{\pi\alpha}{2}\zeta(\alpha)\Gamma(1-\alpha)k^\alpha \\ &+ 4\zeta^2(\alpha-1)k^2 + \mathscr{O}(k^3) \end{aligned} \tag{1.25}$$

In this way, when $\alpha < 1$ and $k \to 0$ the dispersion relation diverges as

$$\lambda_\alpha^\infty(k) \sim 2\Delta\cos\frac{\pi\alpha}{2}\frac{|\Gamma(1-\alpha)|}{|k|^{1-\alpha}}. \tag{1.26}$$

This however gives a finite contribution to the ground-state energy density $e_\infty(\alpha)$ as the integral of $1/|k|^{1-\alpha}$ is finite when $k \to 0$.

From (1.24) we have

$$\begin{aligned} f_\alpha^\infty(k)\frac{\mathrm{d}f_\alpha^\infty(k)}{\mathrm{d}k} &= 4\cos^2\frac{\pi\alpha}{2}\Gamma^2(1-\alpha)(\alpha-1)k^{2\alpha-3} \\ &+ 4\cos\frac{\pi\alpha}{2}\Gamma(1-\alpha)\zeta(\alpha-1)k^\alpha \\ &+ 4\cos\frac{\pi\alpha}{2}\Gamma(1-\alpha)(\alpha-1)\zeta(\alpha-1)k^{\alpha-1} \\ &+ 4\zeta^2(\alpha-1)k^2 + \ldots \end{aligned} \tag{1.27}$$

Then the $k \to 0$ part of the velocity has the following structure (coefficients $A, B, \ldots$ do not depend on k):

$$\frac{\mathrm{d}\lambda_\alpha^\infty(k)}{\mathrm{d}k} = \frac{\left(Ak + Bk^{2\alpha-3} + Ck^\alpha + Dk^{\alpha-1} + Ek^2 + \ldots\right)}{\sqrt{A^2 + Fk^{2\alpha-2} + Gk^\alpha + Hk^2 + \ldots}} \tag{1.28}$$

Let us now distinguish four cases:

(i) $\alpha < 1$: The smallest exponent in the numerator is $2\alpha - 3$ and in the denominator is $2\alpha - 2$, so by collecting these terms one has:

$$\frac{\mathrm{d}\lambda_\alpha(k)}{\mathrm{d}k} = \frac{k^{2\alpha-3}\,(B + \ldots)}{k^{\alpha-1}\,(F + \ldots)^{1/2}} \sim k^{\alpha-2} \to \infty \tag{1.29}$$

which diverges when $k \to 0$ as $\alpha < 1$.

(ii) $1 < \alpha < 3/2$: The smallest exponent in the numerator is still $2\alpha - 3$ while in the denominator is 0 and

$$\frac{\mathrm{d}\lambda_\alpha(k)}{\mathrm{d}k} = \frac{k^{2\alpha-3}\,(B + \ldots)}{(A + \ldots)^{1/2}} \sim k^{2\alpha-3} \to \infty \tag{1.30}$$

which diverges when $k \to 0$ as $1 < \alpha < 3/2$.

(iii) $3/2 < \alpha < 2$: The situation is the same as (ii), but

$$\frac{\mathrm{d}\lambda_\alpha(k)}{\mathrm{d}k} \sim k^{2\alpha-3} \to 0. \tag{1.31}$$

(iv) $\alpha > 2$: The smallest exponent in the numerator is 1 while in the denominator is 0. So

$$\frac{\mathrm{d}\lambda_\alpha(k)}{\mathrm{d}k} \sim k \to 0. \tag{1.32}$$

Thus, if $\mu = 2w$, when $k \to 0$, $\frac{\mathrm{d}\lambda_\alpha(k)}{\mathrm{d}k} \to \infty$ if $\alpha < 3/2$, while $\frac{\mathrm{d}\lambda_\alpha(k)}{\mathrm{d}k} \to 0$ if $\alpha > 3/2$.

Let us now turn to the case $k \to \pi$. $f_\alpha^\infty(\pi)$ never diverges because of the analytic properties of the polylogarithm (see Appendix 1.C)

$$f_\alpha^\infty(k \to \pi) \to -2\mathrm{Li}_{\alpha-1}(-1)(k-\pi) \tag{1.33}$$

and gives for the dispersion relation

$$\lambda_\alpha^\infty(k \to \pi) = 2\Delta|\mathrm{Li}_{\alpha-1}(-1)|(k-\pi) \tag{1.34}$$

a linear behavior with a slope fixing the Fermi velocity v_F:

$$v_F(\alpha) = 2\Delta|\mathrm{Li}_{\alpha-1}(-1)|. \tag{1.35}$$

It is possible now to compute the corrections to the ground state energy density by (1.21):

$\alpha > 3/2$: we have $\lambda_\alpha^{\infty\prime}(0) = 0$, $\lambda_\alpha^{\infty\prime}(\pi) = v_F(\alpha)$ and

$$e_\alpha(L) = e_\alpha^\infty - \frac{\pi v_F(\alpha)}{12L^2} \tag{1.36}$$

so the central charge $c = 1/2$ and the transition is in the same universality class as the Ising model. In this region we can say that the long-range pairing of the Hamiltonian is weak enough not to change the low-energy physics of the model, that can be considered still short range.

$\alpha < 3/2$: we have $\lambda_\alpha^{\infty\prime}(0) \to \infty$ and the corrections to the ground-state energy diverges, too. This signals the breaking of the conformal symmetry of the transition point due to the strong long-range pairing.

A similar result holds for the $\mu = -2w$ line where, if $\alpha > 2$ the correction to the ground state-energy density gives $c = 1/2$ and the model can be consider still short-range, while when $1 < \alpha < 2$, $\lambda_\alpha^{\infty\prime}(0) \to \infty$ and the conformal symmetry of the model is broken[1].

[1] We recall that if $\alpha < 1$ the line $\mu = -2w$ is no more critical.

1.3 Correlation functions

In this section, by exploiting the integrability of Hamiltonian (1.6), we will provide a method for computing the correlation functions. We will find two regions of the phase diagram one in which the correlation functions display a hybrid behavior, the other in which the decays is purely algebraic.

We consider the Green function $g_1(R) = \langle a_R^\dagger a_0 \rangle$ and the anomalous one $g_1^a(R) = \langle a_R^\dagger a_0^\dagger \rangle$ computed on the ground state (1.15). As the model is free, we have also $\langle a_R^\dagger \rangle = \langle a_R \rangle = 0$, so from $g_1(R)$ and $g_2(R)$, all the others correlators can be built by means of Wick's theorem, e.g.

$$\begin{aligned} g_2(R) &= \langle n_R n_0 \rangle \\ &= \langle a_R^\dagger a_R a_0^\dagger a_0 \rangle \\ &= \langle n_R \rangle \langle n_0 \rangle - \langle a_R^\dagger a_0^\dagger \rangle \langle a_R a_0 \rangle + \langle a_R^\dagger a_0 \rangle \langle a_R a_0^\dagger \rangle \end{aligned} \tag{1.37}$$

Let us consider $g_1(R)$. In a finite system one has

$$\langle a_R^\dagger a_0 \rangle = \frac{1}{L} \sum_{n=0}^{L-1} \mathrm{e}^{\mathrm{i} k_n R} \sin^2 \theta_{k_n} = \frac{\delta_{R,0}}{2} - \frac{1}{L} \sum_{n=0}^{L-1} \mathrm{e}^{\mathrm{i} k_n R} \frac{\cos k_n + \mu}{2\lambda_\alpha(k_n)} \tag{1.38}$$

while, in the limit $L \to \infty$ (if $R > 0$)

$$g_1(R) = -\frac{1}{2\pi} \int_0^{2\pi} \mathrm{d}k \, \mathrm{e}^{\mathrm{i} k R} \mathscr{G}_\alpha(k), \tag{1.39}$$

with

$$\mathscr{G}_\alpha(k) = \frac{2w \cos k + \mu}{2\lambda_\alpha^\infty(k)}. \tag{1.40}$$

In the following we will give an asymptotic expansion for (1.39) in the whole phase diagram, and we will find that, for every finite α the integral shows an hybrid decay, e.g. exponential at short distances and algebraic at long distances. The second behavior is unexpected because, in a gapped phase, one expects always an exponential decay [30].

We will find that (1.39) has two main contributions:

(i) the $k \to 0$ part is responsible for the power-law behavior at long distance;

(ii) the $k \to \pi$ part is responsible for the exponential behavior at short distance.

To evaluate the integral, we will use the integration contour in Figure 1.1 and the Cauchy Theorem:

$$g_1(R) = -\frac{1}{2\pi} \lim_{M \to \infty} \left(\int_{\mathscr{C}_0} + \int_{\mathscr{L}_-} + \int_{\mathscr{L}_+} + \int_{\mathscr{C}_{2\pi}} \right) \mathrm{d}z \, \mathrm{e}^{\mathrm{i} z R} \, \mathscr{G}_\alpha(z) \tag{1.41}$$

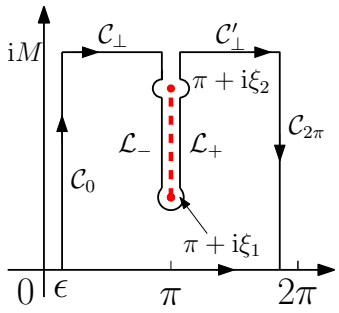

Figure 1.1: Integration contour for evaluating the integral (1.39). The red dashed line is the branch cut of the square root in the denominator of the integrand in (1.39).

with $z = k + iy$. We have neglected the contributions from $\mathscr{C}_\perp$ and $\mathscr{C}'_\perp$ as they vanish when $M \to \infty$.

We choose the $\mathscr{L}_\pm$ contours since the denominator of (1.40), once extended to the complex plane on the line $\pi + iy$, changes its sign since it vanishes for two values $\xi_1 < \xi_2$ given by[2]:

$$(\mu - 2w\cosh\xi_{1,2})^2 + \Delta^2 f_\alpha^\infty(\pi + i\xi_{1,2})^2 = 0 \tag{1.42}$$

The presence of these roots leads to a brach cut for the square root on the line $\pi + iy$. We choose the branch cut in this way:

$$\lambda_\alpha^\infty(z) = \begin{cases} \sqrt{(2w\cosh y - \mu)^2 + \Delta^2 f_\alpha^\infty(\pi + iy)^2} & \text{if } z = \pi + iy \quad y < \xi_1 \text{ or } y > \xi_2 \\ i\sqrt{-(2w\cosh y - \mu)^2 - \Delta^2 f_\alpha^\infty(\pi + iy)^2} & \text{if } z = \pi^+ + iy \quad \xi_1 < y < \xi_2 \\ -i\sqrt{-(2w\cosh y - \mu)^2 - \Delta^2 f_\alpha^\infty(\pi + iy)^2} & \text{if } z = \pi^- + iy \quad \xi_1 < y < \xi_2, \end{cases} \tag{1.43}$$

Let us now analyze the different contributions from the different paths. We shall see that the paths $\mathscr{L}_\pm$ give the exponential decaying part, while $\mathscr{C}_0$ and $\mathscr{C}_{2\pi}$ give the power-law decaying part (at long distances).

Exponential part

On $\mathscr{L}_-$, where $z = \pi^- + iy$ we have[3]

$$\begin{aligned} I_{\mathscr{L}_-} &= -\frac{1}{2\pi}\int_{\mathscr{L}_-} dz\, e^{izR}\,\mathscr{G}_\alpha(z) \\ &= -\frac{ie^{i\pi R}}{2\pi}\int_\infty^{\xi_2} \frac{e^{-yR}(\mu - \cosh y)dy}{\sqrt{(\mu - \cosh y)^2 + f_\alpha^2(\pi + iy)}} \\ &\quad - \frac{ie^{i\pi R}}{2\pi}\int_{\xi_2}^{\xi_1} \frac{e^{-yR}(\mu - \cosh y)dy}{-i\sqrt{-(\mu - \cosh y)^2 - f_\alpha^2(\pi + iy)}} \end{aligned} \tag{1.44}$$

[2] We notice that $f_\alpha^2(\pi + iy)$ is real.

[3] In this section we set $2w = \Delta = 1$.

where we choose the right expression for the square root, according to (1.43).

In the same way, on $\mathscr{L}_+$, we have

$$\begin{aligned} I_{\mathscr{L}_+} &= \frac{\mathrm{i}e^{\mathrm{i}\pi R}}{2\pi}\int_{\xi_2}^{\infty} e^{-yR}\mathscr{G}_\alpha(\pi^+ + \mathrm{i}y)\mathrm{d}y \\ &+ \frac{\mathrm{i}e^{\mathrm{i}\pi R}}{2\pi}\int_{\xi_1}^{\xi_2} e^{-yR}\mathscr{G}_\alpha(\pi^+ + \mathrm{i}y)\mathrm{d}y \end{aligned} \tag{1.45}$$

and, because of the two expressions for $\lambda_\alpha^\infty(\pi^\pm + \mathrm{i}y)$ when $z = \pi^\pm + \mathrm{i}y$ from equation (1.43), $I_{\mathscr{L}_-} + I_{\mathscr{L}_+}$ shows an exponential decay with an inverse correlation length given by ξ_1:

$$\begin{aligned} I_{\mathscr{L}_-} + I_{\mathscr{L}_+} &= \frac{\mathrm{i}e^{\mathrm{i}\pi R}}{\pi}\int_{\xi_1}^{\xi_2} \mathrm{d}y\, e^{-yR}\mathscr{G}_\alpha(\pi^+ + \mathrm{i}y) \\ &= \frac{\mathrm{i}e^{\mathrm{i}\pi R}}{\pi}e^{-\xi_1 R}\int_0^{\xi_2} \mathrm{d}y\, e^{-yR}\mathscr{G}_\alpha(\pi^+ + \mathrm{i}(y+\xi_1)). \end{aligned} \tag{1.46}$$

The previous integral is a Laplace-type integral [47]. We can get its leading behavior, first by replacing ξ_2 with infinity, as the integrand is exponentially suppressed and then by integrating the $y \to 0$ part of $\mathscr{G}_\alpha(\pi^+ + \mathrm{i}(y+\xi_1))$. One has

$$\mathscr{G}_\alpha(\pi^+ + \mathrm{i}(y+\xi_1)) \sim \frac{A_\alpha(\mu)}{\mathrm{i}\sqrt{y}} \quad \text{if } y \to 0 \tag{1.47}$$

with

$$A_\alpha(\mu) = \frac{\mu - \cosh\xi_1}{2\sqrt{2}[\mathrm{Li}_{\alpha-1}(-e^{\xi_1}) + \mathrm{Li}_{\alpha-1}(-e^{-\xi_1})]^{1/2}[\mathrm{Li}_\alpha(-e^{\xi_1}) - \mathrm{Li}_\alpha(-e^{-\xi_1})]^{1/2}} \tag{1.48}$$

so

$$I_{\mathscr{L}_-} + I_{\mathscr{L}_+} = A_\alpha(\mu)\frac{e^{\mathrm{i}\pi R}}{\sqrt{\pi}}\frac{e^{-\xi_1 R}}{\sqrt{R}} \tag{1.49}$$

showing the exponential decay.

Power-law part

On $\mathscr{C}_0$, $z = \epsilon + \mathrm{i}y$ (ϵ is an infinitesimal parameter we let it go to zero) we have

$$\begin{aligned} I_{\mathscr{C}_0} &= -\frac{1}{2\pi}\int_{\mathscr{C}_0} e^{\mathrm{i}zR}\,\mathscr{G}_\alpha(z)\mathrm{d}z \\ &= -\frac{\mathrm{i}}{2\pi}\int_0^{\infty} e^{-yR}\,\mathscr{G}_\alpha(\epsilon + \mathrm{i}y)\mathrm{d}y \end{aligned} \tag{1.50}$$

while on $\mathscr{C}_{2\pi}$, $z = 2\pi - \epsilon + \mathrm{i}y$

$$\begin{aligned} I_{\mathscr{C}_{2\pi}} &= -\frac{1}{2\pi}\int_{\mathscr{C}_{2\pi}} \mathrm{e}^{\mathrm{i}zR}\,\mathscr{G}_\alpha(z)\mathrm{d}z \\ &= \frac{\mathrm{i}}{2\pi}\int_0^\infty \mathrm{e}^{-yR}\,\mathscr{G}_\alpha(2\pi-\epsilon+\mathrm{i}y)\mathrm{d}y \end{aligned} \tag{1.51}$$

Now, as $\mathscr{G}_\alpha(2\pi - \epsilon + \mathrm{i}y) = \mathscr{G}^*_\alpha(\epsilon + \mathrm{i}y)$

$$\begin{aligned} I_{\mathscr{C}_0} + I_{\mathscr{C}_{2\pi}} &= \frac{1}{\pi}\int_0^\infty \mathrm{d}y\,\mathrm{e}^{-yR}\,\mathrm{Im}(\mathscr{G}_\alpha(\epsilon+\mathrm{i}y)) \\ &= \frac{1}{\pi}\int_0^\infty \mathrm{d}y\,\mathrm{e}^{-yR}\,\mathrm{Im}(\mathscr{G}_\alpha(\mathrm{i}y)) \end{aligned} \tag{1.52}$$

where in the last equation we let $\epsilon \to 0$.

The integral in (1.52) is the Laplace transform of $\mathscr{G}_\alpha(\mathrm{i}y))$, so we can evaluate its asymptotic behavior, as we did before, by computing the $y \to 0$ part of $\mathscr{G}_\alpha(\mathrm{i}y))$ and then integrating [47]. In the following we will consider the case of $\alpha \neq 1, 2, \ldots$ where we can use the series expansion of the polylogarithm

$$\mathrm{Li}_\alpha(\mathrm{e}^{\pm y}) = -\Gamma(1-\alpha)(\mp y)^{\alpha-1} + \sum_{j=0}^\infty \frac{\zeta(\alpha-j)}{j!}(\pm y)^j. \tag{1.53}$$

Now

$$\begin{aligned} \mathrm{Li}_\alpha(\mathrm{e}^y) - \mathrm{Li}_\alpha(\mathrm{e}^{-y}) &= -\Gamma(1-\alpha)\left(\mathrm{e}^{\mathrm{i}\pi\alpha}+1\right)y^{\alpha-1} \\ &\quad + 2\sum_{j=0}^\infty \frac{\zeta(\alpha-(2j+1))}{(2j+1)!}y^{2j+1} \end{aligned} \tag{1.54}$$

and the main contribution to the imaginary part of $\mathscr{G}_\alpha(\mathrm{i}y)$, due to $\mathrm{Li}_\alpha(\mathrm{e}^y)$, is given by

$$\mathscr{G}_\alpha(\mathrm{i}y) \sim \frac{\mu+1}{2\sqrt{(\mu+1)^2 - \Gamma^2(1-\alpha)(\mathrm{e}^{\mathrm{i}\pi\alpha}+1)^2 y^{2\alpha-2} + 4\Gamma(1-\alpha)(\mathrm{e}^{\mathrm{i}\pi\alpha}+1)\zeta(\alpha-1)y^\alpha}} \tag{1.55}$$

We have now to distinguish three cases $\alpha > 2$, $1 < \alpha < 2$ and $\alpha < 1$.

$\alpha > 2$: The Taylor expansion of (1.55), as the leading power in the denominator is y^α, is:

$$\mathscr{G}_\alpha(\mathrm{i}y) \sim \frac{\mathrm{sgn}\,(\mu+1)}{2}\left(1 - 2\frac{\Gamma(1-\alpha)(\mathrm{e}^{\mathrm{i}\pi\alpha}+1)\zeta(\alpha-1)y^\alpha}{(\mu+1)^2}\right) \tag{1.56}$$

and its imaginary part

$$\operatorname{Im}\mathscr{G}_\alpha(\mathrm{i}y) \sim -\frac{\Gamma(1-\alpha)\sin(\pi\alpha)\zeta(\alpha-1)y^\alpha}{\operatorname{sgn}(\mu+1)(\mu+1)^2}. \tag{1.57}$$

entering eq.(1.52) gives

$$\begin{aligned} I_0 + I_{2\pi} &= -\frac{\zeta(\alpha-1)\Gamma(1-\alpha)\sin(\pi\alpha)}{\pi\operatorname{sgn}(\mu+1)(1+\mu)^2}\int_0^\infty \mathrm{d}y\,\mathrm{e}^{-yR}y^\alpha \\ &= -\frac{\zeta(\alpha-1)\Gamma(1-\alpha)\Gamma(\alpha+1)\sin(\pi\alpha)}{\pi\operatorname{sgn}(\mu+1)(1+\mu)^2}\frac{1}{R^{\alpha+1}} \\ &= -\frac{\alpha\zeta(\alpha-1)}{\operatorname{sgn}(\mu+1)(1+\mu)^2}\frac{1}{R^{\alpha+1}} \end{aligned} \tag{1.58}$$

where we used Euler's reflection formula $\Gamma(\alpha)\Gamma(1-\alpha) = \pi/\sin(\pi\alpha)$ to extend the previous equation to integer α also.

$1 < \alpha < 2$: The leading contribution to the denominator of $\mathscr{G}_\alpha(y)$ is $y^{2\alpha-2}$ and one has:

$$\mathscr{G}_\alpha(\mathrm{i}y) \sim \frac{\operatorname{sgn}(\mu+1)}{2}\left(1+\frac{\Gamma(1-\alpha)^2(\mathrm{e}^{\mathrm{i}\pi\alpha}+1)^2y^{2\alpha-2}}{2(\mu+1)^2}\right) \tag{1.59}$$

having imaginary part

$$\operatorname{Im}\mathscr{G}_\alpha(\mathrm{i}y) \sim \frac{\Gamma(1-\alpha)^2\sin(\pi\alpha)\cos^2\left(\frac{\pi\alpha}{2}\right)y^{2\alpha-2}}{\operatorname{sgn}(\mu+1)(\mu+1)^2}. \tag{1.60}$$

So,

$$\begin{aligned} I_0 + I_{2\pi} &= \frac{\Gamma(1-\alpha)^2\sin(\pi\alpha)\cos^2\left(\frac{\pi\alpha}{2}\right)}{\pi\operatorname{sgn}(\mu+1)(\mu+1)^2}\int_0^\infty \mathrm{d}y\,\mathrm{e}^{-yR}y^{2\alpha-2} \\ &= \frac{\Gamma(1-\alpha)^2\sin(\pi\alpha)\cos^2\left(\frac{\pi\alpha}{2}\right)\Gamma(2\alpha-1)}{\pi\operatorname{sgn}(\mu+1)(\mu+1)^2}\frac{1}{R^{2\alpha-1}}. \end{aligned} \tag{1.61}$$

$\alpha < 1$: By multiplying both the denominator and the numerator of $\mathscr{G}_\alpha(\mathrm{i}y)$ in (1.55) by $y^{1-\alpha}$ and then by Taylor expanding we have

$$\operatorname{Im}\mathscr{G}_\alpha(\mathrm{i}y) \sim \frac{(\mu+1)}{4\Gamma(1-\alpha)}y^{1-\alpha} \tag{1.62}$$

and

$$\begin{aligned} I_{\mathscr{C}_0} + I_{\mathscr{C}_{2\pi}} &= \frac{(\mu+1)}{2\pi\Gamma(1-\alpha)}\int_0^\infty \mathrm{d}y\,y^{1-\alpha}\,\mathrm{e}^{-yR} \\ &= \frac{(\mu+1)(1-\alpha)}{4\pi}\frac{1}{R^{2-\alpha}} \end{aligned} \tag{1.63}$$

By collecting all the contributions, we found that

$$\begin{aligned}\langle a_R^\dagger a_0\rangle = &\frac{A_\alpha(\mu)\mathrm{e}^{\mathrm{i}\pi R}}{\sqrt{\pi}}\frac{\mathrm{e}^{-\xi_1 R}}{\sqrt{R}}\\ &-\frac{\alpha\zeta(\alpha-1)}{\operatorname{sgn}(\mu+1)(1+\mu)^2}\frac{1}{R^{\alpha+1}}\quad \text{for } \alpha>2,\end{aligned}\tag{1.64}$$

$$\begin{aligned}\langle a_R^\dagger a_0\rangle = &\frac{A_\alpha(\mu)\mathrm{e}^{\mathrm{i}\pi R}}{\sqrt{\pi}}\frac{\mathrm{e}^{-\xi_1 R}}{\sqrt{R}}\\ &+\frac{\Gamma(1-\alpha)^2\sin(\pi\alpha)\cos^2\left(\frac{\pi\alpha}{2}\right)}{\pi\operatorname{sgn}(\mu+1)(\mu+1)^2}\frac{\Gamma(2\alpha-1)}{R^{2\alpha-1}}\quad \text{for } 1<\alpha<2\end{aligned}\tag{1.65}$$

and

$$\begin{aligned}\langle a_R^\dagger a_0\rangle = &\frac{A_\alpha(\mu)\mathrm{e}^{\mathrm{i}\pi R}}{\sqrt{\pi}}\frac{\mathrm{e}^{-\xi_1 R}}{\sqrt{R}}\\ &+\frac{(\mu+1)(1-\alpha)}{4\pi}\frac{1}{R^{2-\alpha}}\quad \text{for } \alpha<1\end{aligned}\tag{1.66}$$

where $A_\alpha(\mu)$ is given by (1.48) and ξ_1 is the smallest solution of

$$(\mu-\cosh\xi_{1,2})^2-\left(\mathrm{Li}_\alpha(-\mathrm{e}^{-\xi_{1,2}})-\mathrm{Li}_\alpha(-\mathrm{e}^{\xi_{1,2}})\right)^2=0.\tag{1.67}$$

In Fig. 1.2 the comparison between the exact integral (1.39) and equation (1.64) is reported. One can see that the power-law tail occurs when the two contributions in (1.64) and (1.65) become of the same order of magnitude. This usually happens when $\alpha>1$.

When $\alpha<1$ one can show, numerically, that even if equation (1.42) has one or two solutions, the exponential part in (1.66) is negligible with respect to the power-law tail. This gives a pure power-law correlation function.

Fig. 1.3(a) shows the decaying exponent computed numerically from (1.39) and compared with eqs. (1.64), (1.65), (1.66).

1.3.1 Anomalous correlator

The correlators $g_1^a(R)=\langle a_R^\dagger a_0^\dagger\rangle$ is given by

$$\begin{aligned}\langle a_R^\dagger a_0^\dagger\rangle &= \frac{1}{L}\sum_{n=0}^{L-1}\mathrm{e}^{\mathrm{i}k_n R}\,\mathrm{i}\sin\theta_{k_n}\cos\theta_{k_n}\\ &= \frac{\mathrm{i}}{L}\sum_{n=0}^{L-1}\mathrm{e}^{\mathrm{i}k_n R}\frac{\Delta f_\alpha(k_n)}{2\lambda_\alpha(k_n)}\end{aligned}\tag{1.68}$$

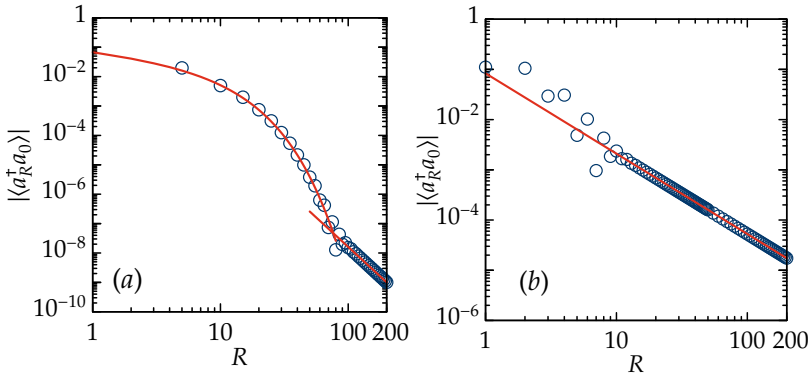

Figure 1.2: Panel (a) integral (1.39) (points) and eq. (1.64) (solid line) for $\alpha = 3$ and $\mu = 0.75$. Panel (b) integral (1.39) (points) and eq. (1.66) (solid line) for $\alpha = 0.4$ and $\mu = 0.75$ showing the exact matching between analytics and numerics.

in a finite system, while, in the thermodynamic limit

$$\langle a_R^\dagger a_0^\dagger\rangle = \frac{1}{2\pi}\int_0^{2\pi} \mathrm{e}^{\mathrm{i}kR}\,\mathscr{F}_\alpha(k) \tag{1.69}$$

with

$$\mathscr{F}_\alpha(k) = \mathrm{i}\frac{\Delta f_\alpha^\infty(k)}{2\lambda_\alpha^\infty(k)}. \tag{1.70}$$

Using the same integration contour as before we get for $g_1^a(R)$

$$\begin{aligned}\langle a_R^\dagger a_0^\dagger\rangle = {} & \frac{\mathrm{e}^{\mathrm{i}\pi R}\mathrm{e}^{-\xi_1 R}}{\pi}\int_0^\infty \mathrm{d}y\,\mathrm{e}^{-yR}\mathscr{F}_\alpha(\pi^+ + \mathrm{i}(y+\xi_1)) \\ & - \frac{1}{\pi}\int_0^\infty \mathrm{d}y\,\mathrm{e}^{-yR}\,\mathrm{Im}\,\mathscr{F}_\alpha(\mathrm{i}y)\end{aligned} \tag{1.71}$$

showing both the exponential and the power law contributions. ξ_1 is always the smallest solution of[4]

$$(\mu - \cosh\xi_{1,2})^2 - \left(\mathrm{Li}_\alpha(-\mathrm{e}^{-\xi_{1,2}}) - \mathrm{Li}_\alpha(-\mathrm{e}^{\xi_{1,2}})\right)^2 = 0. \tag{1.72}$$

If $\alpha > 1$, as

$$\mathrm{Im}\,\mathscr{F}_\alpha(\mathrm{i}y) \sim \frac{\Gamma(1-\alpha)\sin\pi\alpha}{2|\mu+1|}y^{\alpha-1} \tag{1.73}$$

we have

$$\langle a_R^\dagger a_0^\dagger\rangle = \frac{B_\alpha(\mu)\mathrm{e}^{\mathrm{i}\pi R}}{\sqrt{\pi}}\frac{\mathrm{e}^{-\xi_1 R}}{\sqrt{R}} - \frac{1}{2|\mu+1|}\frac{1}{R^\alpha} \tag{1.74}$$

[4]From now and to the end of this section we use $\Delta = 2w = 1$

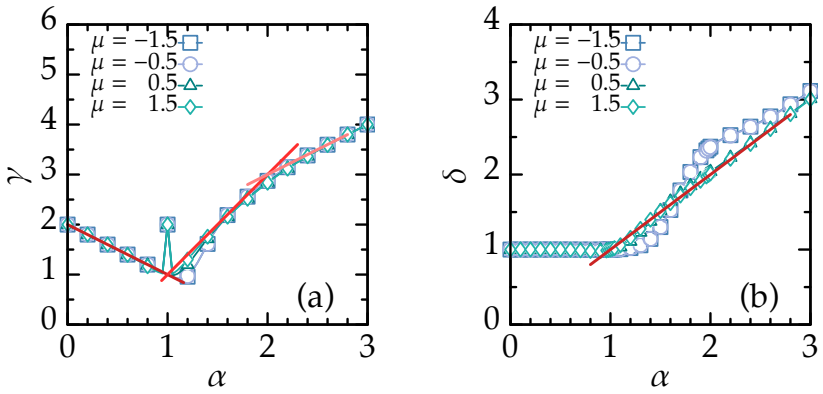

Figure 1.3: (a) Decay exponent of (1.39) compared with eqs. (1.64), (1.65), (1.66). The equations of the three straight lines are $2-\alpha$, $2\alpha-1$ and $\alpha+1$. The point $\alpha=1$ is discussed in Appendix 1.C. (b) Decay exponent of (1.69). The equation of the straight line is α. The discrepancy between the fitted values and the analytical line is due to numerical errors.

with

$$B_\alpha(\mu)=\frac{[\mathrm{Li}_\alpha(-e^{\xi_1})-\mathrm{Li}_\alpha(-e^{-\xi_1})]^{1/2}}{2\sqrt{2}[\mathrm{Li}_{\alpha-1}(-e^{\xi_1})+\mathrm{Li}_{\alpha-1}(-e^{-\xi_1})]^{1/2}} \tag{1.75}$$

while, if $\alpha<1$

$$\mathrm{Im}\,\mathscr{F}_\alpha(iy)\sim\frac{1}{2} \tag{1.76}$$

and

$$\langle a_R^\dagger a_0^\dagger\rangle=\frac{B_\alpha(\mu)e^{i\pi R}}{\sqrt{\pi}}\frac{e^{-\xi_1 R}}{\sqrt{R}}-\frac{1}{2\pi}\frac{1}{R}. \tag{1.77}$$

Fig. 1.3(b) shows the comparison between the fitted exponent from (1.69) and the analytical results in (1.74) and (1.77).

From $g_1(R)$ and $g_1^a(R)$ one can compute the connected two-point correlation function $g_2^c(R)=\langle n_R n_0\rangle-\langle n_R\rangle\langle n_0\rangle$ that behaves as $g_2^c(R)\sim 1/R^{2\alpha}$ when $\alpha>1$. The the decaying exponent we found is the same as the one of the Ising model numerically computed in [48].

1.4 Entanglement scaling

In recent years, entanglement measures have been used to characterize the properties of a quantum many-body system [49–57].

At zero temperature, the system occupies the ground state $|GS\rangle$ of a Hamiltonian H and $|GS\rangle$ contains all the information on the static properties that can be readily collected by an entanglement measure on it. Entanglement can provide also a practical way to detect the boundaries [58] between different phases, since it is sensitive to the presence of critical points

of quantum phase transitions. Mreover the final efficiency of numerical techniques, based e.g. on density matrix renormalization group and similar methods, for approximating a quantum state, is related to the amount of entanglement of such a state [59]. A good control on it can give very good quasi-exact approximations.

A measure of the rate of entanglement present in $|GS\rangle$ can be given by the von-Neumann entropy S_{vN} we will introduce in the following.

Let us consider a one-dimensional chain of length L, and a partition into two disjoint subsystems A and B containing ℓ and $L-\ell$ sites, respectively.

We can build the density matrix of the total system through $|GS\rangle$

$$\rho = |GS\rangle\langle GS| \tag{1.78}$$

and we can define the reduced density matrix for subsystem A tracing out the degrees of freedom of B from the total ρ:

$$\rho_A(\ell) = \text{Tr}_B\, \rho \tag{1.79}$$

so we can look at the subsystem A to be in a mixed state defined by the previous ρ_A.

The von Neumann entanglement entropy S_{vN} is defined as the entropy of the reduced density matrix ρ_A

$$S_{\text{vN}}(\ell) = -\text{Tr}\, \rho_A \log_2 \rho_A \tag{1.80}$$

We are interested in the the scaling of the entanglement $S_{\text{vN}}(\ell)$ with the sub-system size ℓ.

By recalling the thermodynamic concept of entropy[5], being an extensive quantity, it obeys a *volume law*, and one could think that even S_{vN} has an extensive behavior.

This is, however, not true for ground states of gapped local Hamiltonians and one generally finds they obey an *area law* [60], meaning that, for one-dimensional systems, the entropy saturates to a constant.

Moreover, it has been shown that, the scaling changes at criticality and reflects the universal behavior of the system, making the measure of entanglement a powerful method for getting information on the universality properties of critical points [31, 61].

For one-dimensional systems with local Hamiltonian defined on a ring of length L, these two different behaviors can be summarized as follows:

(i) At criticality $S_{\text{vN}}(\ell)$ diverges logarithmically with the block size ℓ

$$S_{\text{vN}}(\ell) = \frac{c}{3}\log_2\left[\frac{L}{\pi}\sin\left(\frac{\pi\ell}{L}\right)\right] + a \tag{1.81}$$

[5]Thermal entropy has the same functional form as (1.80) with ρ_A the canonical or gran-canonical density matrix.

where c is the central charge of the underlying conformal field theory and a is a nonuniversal constant.

This scaling can be used to compute the central charge c of the theory also for non-integrable model, by employing, e.g. DMRG techniques [62–64] that can directly access to the reduced density matrix $\rho_A(\ell)$ and, then, to $S_{\text{vN}}(\ell)$.

(ii) Away from criticality, where the system has a gap and because of this a finite correlation length ξ [65] the entropy saturates to a constant

$$S_{\text{vN}}(\ell) = \frac{c}{3} \log_2 \xi \tag{1.82}$$

and obeys an area law.

In this section we will compute the von Neumann entropy $S_{\text{vN}}(\ell)$ for the Hamiltonian (1.6) by exploiting the method of Appendix 1.B as H in (1.6) is quadratic.

For different system sizes L and for different values of μ (fixing in this section $\Delta = 2w = 1$) and α, we computed the entropy $S_{\text{vN}}(L/2)$ for half of the chain. Then, to study where a violation of the area law occurs (*i.e.* when the entropy does not saturate to a constant), we used eq. (1.81), in principle valid only where the system is critical, to define an effective central charge c_{eff} throughout the all phase diagram

$$S_{\text{vN}}(\ell) = \frac{c_{\text{eff}}}{3} \log_2 \left[\frac{L}{\pi} \sin\left(\frac{\pi \ell}{L} \right) \right] + a \tag{1.83}$$

in analogy of what has been done for the Ising model with long-range interactions in [48].

Figure 1.4 shows the plots of $S_{\text{vN}}(L/2)$ opportunely rescaled both for a gapped and a critical point, while the resulting c_{eff} is reported in Figure 1.5.

What we found is that

(i) for $\alpha > 1$, $c_{\text{eff}} = 0$ almost everywhere in the gapped region $|\mu| \neq 2w$. This is equivalent to say that the area law is not violated and the scaling of the entropy does not depend on the system size;

(ii) for $\alpha < 1$, $c_{\text{eff}} \neq 0$ within the gapped region. This corresponds to the violation of the area law and it is unexpected if the phase is gapped, because of (1.82). The behavior of c_{eff}, as well as of the correlation functions discussed before, can be ascribed to the very strong long-range pairing, showing up in non-local quantities such as $S_{\text{vN}}(L/2)$ and correlation functions.

A cut of the phase diagram of Figure 1.5, for $\mu = 0.5$ e $\mu = 1$ is shown in Figure 1.6, where one can see the increasing of the central charge on the critical line, and the violation of the area law in the gapped phase.

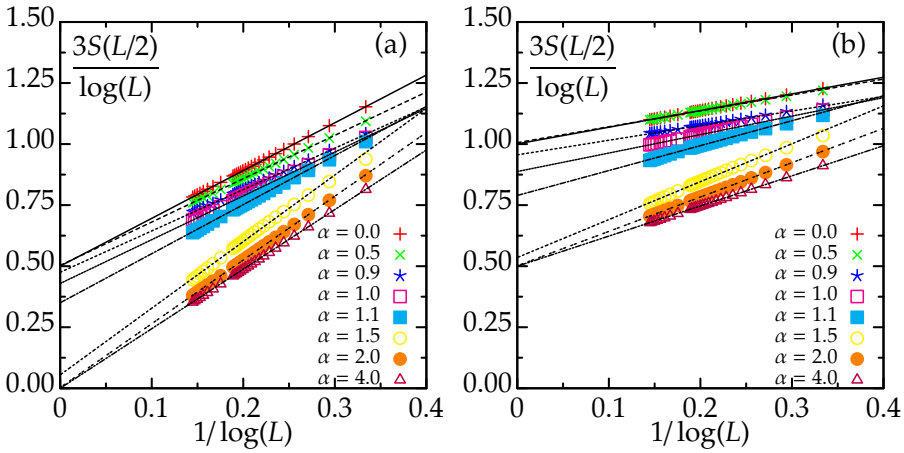

Figure 1.4: The plots show the values of $S_{\mathrm{vN}}(L/2)$ (rescaled in order to easily read from the y-axis the value of c_{eff}) for (a) the gapped point $\mu = 0.5$ and (b) the critical point $\mu = 1$ as function of $1/\log_2(L)$. The intercept on the y-axis gives c_{eff} in the thermodynamic limit. One can see that by decreasing α, for a gapped point (a), c_{eff} goes from 0 (short-range regime) to 1/2 (area law violation), while for a critical point (b), c_{eff} goes from 1/2 (as expected for the XY-Ising model) to 1.

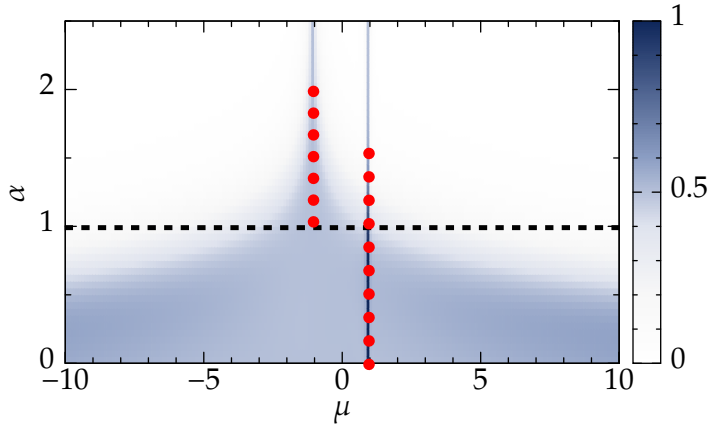

Figure 1.5: Phase diagram obtained through the effective central charge c_{eff} by fitting the von Neumann entropy $S(L/2)$. Two gapless conformal field theories with $c = 1/2$ are visible for $\mu = 1$ ($\alpha > 3/2$) and $\mu = -1$ ($\alpha > 2$). Red vertical dotted lines: gapless lines with broken conformal symmetry. Horizontal dashed line separates two regions: correlation functions display a hybrid exponential-algebraic ($\alpha > 1$) and purely algebraic decay ($\alpha < 1$).

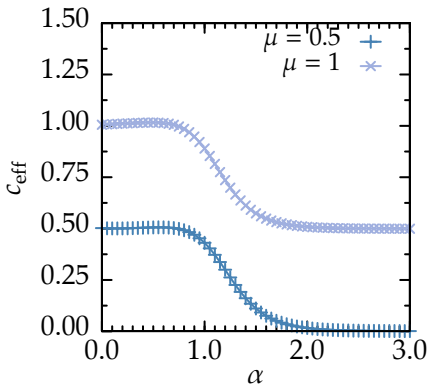

Figure 1.6: The plot shows both the violation of the area law in the gapped phase ($\mu = 0.5$) when $\alpha < 1$ and the increasing of the central charge (from $1/2$ to 1) when α decreases to 0 on the critical line $\mu = 1$.

Let us discuss the behavior of the central charge on the critical line $\mu = 1$. We have seen that the finite size corrections to the ground state energy diverge for $\alpha < 3/2$, while here we found $c > 1/2$ for $\alpha < 3/2$ (Figure 1.6) to arrive to $c = 1$ for $\alpha = 0$. This value is the same as a Luttinger liquid and it would correspond to a conformal bosonic theory. These two theories (Ising with $c = 1/2$ and Luttinger $c = 1$), are described by two completely different conformal field theories, the principal difference being the number of primary fields they admit. For a complete review one can see [37, 66–68].

In particular, the degeneracy patterns of the excited states have two different behaviors.

If we take into account the Ising model, the excitations can be made up by constructing a multi-particle state and adding the required combinations of single-particle energy given by

$$\lambda(k_n) = \sqrt{(\cos k_n - 1)^2 + \gamma^2 \sin^2 k_n} \tag{1.84}$$

at criticality, with $k_n = 2\pi(n+1/2)/L$. We note that, as the dispersion relation is symmetric with respect to $k = 0$ there are two fermions with opposite momenta carrying the same energy.

Consider now, the single particle low-lying excitations. The are created near $k = 0$ and their energy, in the limit of a long, but finite chain is

$$\lambda(k_n) = v_F \frac{2\pi}{L} \left| n + \frac{1}{2} \right| \text{ with } k_n \sim 0 \tag{1.85}$$

with $v_F = \gamma$ the Fermi velocity (see eq. (1.159)).

n	0	1	2	3	4	5
$\mathscr{E}_n^{\text{even}}$	0	1	2	3	4	5
degeneracy	1	1	4	5	9	13

n	1	2	3	4	5
$\mathscr{E}_n^{\text{odd}}$	1/2	3/2	5/2	7/2	9/2
degeneracy	2	2	4	6	12

Table 1.1: Degeneracies of the even (upper table) and odd-particle (lower table) sectors of the Ising model. The same degeneracies are found for the long-range Hamiltonian both for $\alpha > 1$ and for $\alpha < 1$ (see Figure 1.7).

If we rescale energy and momentum, by defining

$$\epsilon_n = \frac{L}{2\pi v_F}\lambda(k_n) = \left|n + \frac{1}{2}\right| \tag{1.86}$$

$$p_n = n + \frac{1}{2} \tag{1.87}$$

the low-lying excitations are given by choosing n between $0, \pm 1, \pm 2 \ldots$ and recalling that, as the theory is fermionic, we cannot have two fermions with the same quantum number.

Now we can divide the excitations into two groups as they can be given by an odd or an even number of fermions and then we count their degeneracies.

Let us consider the odd-particle number excitations. The first excitation will be given by $n = 0$ with momentum $p_0 = 1/2$ and $\mathscr{E}_1^{\text{odd}} = \epsilon_0 = 1/2$.

The second one, if we consider $n = -1$ will have always an energy $\epsilon_{-1} = 1/2$, but an opposite momentum $p_{-1} = -1/2$, so it will be degenerate with the first.

The next energy level $\mathscr{E}_2^{\text{odd}} = 3/2$ will be always two-fold degenerate, because it can be given by $n = 1$, or $n = -2$. The case $\mathscr{E}_3^{\text{odd}} = 5/2$ is different, as this can be built directly with a particle in $n = 2$ ($p_2 = 3/2$) or $n = -3$ ($p_{-3} = -3/2$) or with three particles in $\{n_1 = 0, n_2 = -1, n_3 = 2\}$ (with total momentum $p_0 + p_{-1} + p_2 = 5/2$) or $\{n_1 = 0, n_2 = -1, n_3 = -3\}$ (with momentum $-5/2$) and it will be four-fold degenerate.

In the same way, one can compute all the degeneracy pattern also in the even sector. Table 1.1 shows the degeneracies of the first levels both for the odd and for the even particle sectors of the Ising model [37].

If we now compute the degeneracy of the long-range Hamiltonian (1.6) we will always find the previous patterns, no matter which α we consider, as the theory has always fermionic excitations. They are shown in Figure 1.7.

We can thus conclude, that the entanglement entropy cannot be used to probe the fermionic character of (1.6) as the conformal field theory is broken

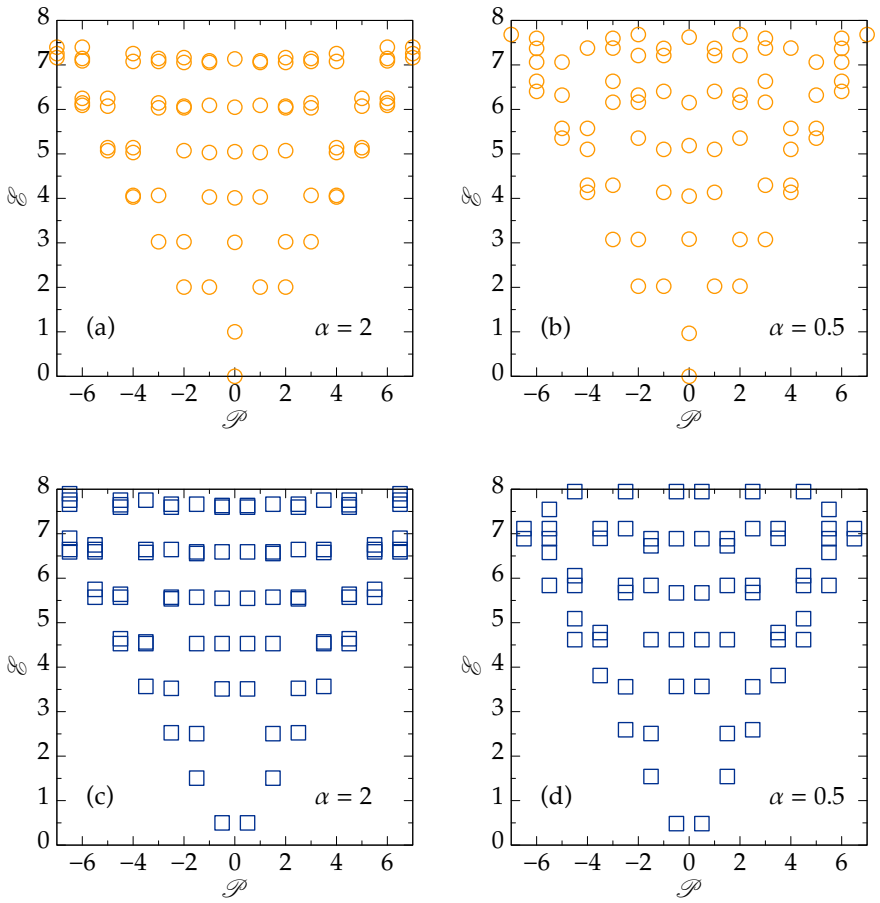

Figure 1.7: Degeneracy patterns for the long-range Hamiltonian for different α at criticality. (a), (b) panels for the excitations with an even particle number, (c), (d) for the excitations with an odd number of particles. The two plots show the same degeneracies as a $c = 1/2$ theory reported in Table 1.1.

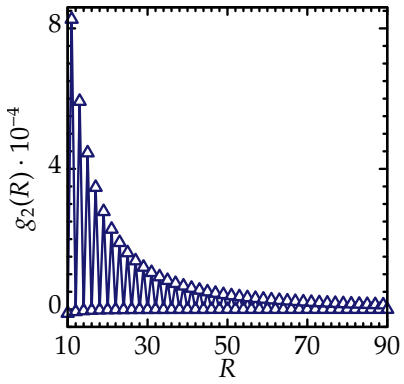

Figure 1.8: The plot shows the density-density correlation function $g_2(R)$ at $\mu = 1$, $\alpha = 0$ with a dimerized behavior, responsible for the doubling of the central charge on the critical line.

and the entanglement scaling of (1.81), which was derived in a conformal field theory context, does not hold.

We can however explain the apparent doubling of the central charge by looking at the correlation functions used to compute the von Neumann entropy. Using the technique of the previous section we can compute the density-density correlation function, for $\alpha = 0$, that comes out to be (Figure 1.8)

$$g_2(R) = \frac{1 - \cos \pi R}{2\pi^2 R^2} \tag{1.88}$$

which is identical to the one of a Luttinger liquid yielding for the central charge the value $c = 1$ [69].

1.5 Entropy scaling after a quench

The breaking of the conformal field theory on the critical line $\mu = 2w$ for sufficiently small $\alpha < 1$, discussed in the previous section, can be tested by looking at the scaling of the entanglement entropy after a global quench.

In recent years, the time evolution in of entanglement measures has been investigated both analytically [38, 70–75] and numerically [39, 76–79], even because the growth in time of the entanglement between two halves of a many-body system takes into account the quantum correlations between them and, from a numerical point of view, it can give information on the complexity of the numerical approximation of this system, when using, for example, matrix product state representation [80–83]

A global quench is a changing of one or more parameters in the system, previously prepared in a given state $|\psi\rangle$ (that can be taken as the ground state of a pre-quench Hamiltonian H_0) that, for $t > 0$ is allowed to evolve with a different post-quench Hamiltonian H_1.

Let us briefly review what is the entanglement dynamics for a system with short range interactions, for which we will employ the so-called semiclassical approximation [70] for the quench dynamics, valid when the post-quench Hamiltonian can be written in terms of free-moving particles.

We will get an estimation of the rate of the growth of the entanglement $S(t)$ between two parts A (of length ℓ) and B of the system.

As soon as the evolution, ruled by the post-quench Hamiltonian H_1, starts, we have the instantaneous production of pairs of quasi-particles with opposite momenta k and $-k$, created somewhere in the system. These are entangled pairs and they move freely in the system with a finite group velocity v_g.

The maximum for the group velocity was theoretically studied in [84] and, for a system with short range interactions always exists. It is given by the Lieb-Robinson bound which also defines an effective light cone outside of which correlations are exponentially suppressed.

Now, quasiparticles created in A arriving in B entangle the two parts and, as the rate of arrival in B is constant (v_g being constant) the entropy between A and B grows linear in time. This was also proven for a quench in a conformal field theory in [38] where a universal behavior for $S(t)$ was found

$$S(t) = \begin{cases} \dfrac{\pi c t}{6} & t < \ell/2 \\ \dfrac{\pi c \ell}{12} & t > \ell/2 \end{cases} \tag{1.89}$$

In the case of long-range interactions with power α, where the Lieb-Robison bound has to be modified to take them into account [85], more regimes were found for the spreading of correlations and entanglment entropy [39, 75, 77, 86, 87].

In particular for the Ising model with long range interactions three different regimes for the entanglement were identified [39]

(i) for relatively short-range interactions ($\alpha > 1$), entropy grows linearly in time as explained before with the semiclassical picture;

(ii) for long-range interactions $\alpha \sim 0.8, 0.9, 1$ the half-chain entanglement entropy grows logarithmically;

(iii) for strong long-range interactions $\alpha \lesssim 0.2$, rapid oscillations of the half-chain entanglement entropy were observed around small values.

We studied, in this work, the entanglement growth after a quench ruled by the Hamiltonian (1.6) for different α (with $\Delta = 2w = 1$), by using the following quench protocol.

We prepared the system in $|\psi^{(0)}\rangle$ that is the ground state of (1.6) when $\mu_0 \gg 1$. This state is characterized by a Bogolyubov angle $\theta^{(0)}_{q_n}$ given by

(1.12). Then we let $|\psi^{(0)}\rangle$ evolve by means of $H^{(1)}$ eq. (1.6) with $\mu_1 = 1$:

$$|\psi(t)\rangle = \mathrm{e}^{-\mathrm{i}H^{(1)}t}\,|\psi^{(0)}\rangle\,. \tag{1.90}$$

We will measure time t in unit of $\hbar/J$ where J is the energy scale used for the Hamiltonian $H^{(1)}$.

$H^{(1)}$ can be written in a new Bogolyubov basis corresponding to a Bogolyubov angle $\theta^{(1)}_{q_n}$ and it takes the form

$$H^{(1)} = \sum_{n=0}^{L-1} \lambda^{(1)}_{\alpha}(q_n)\left(\eta^{(1)\dagger}_{k_n}\eta^{(1)}_{q_n} - \frac{1}{2}\right) \tag{1.91}$$

with

$$\lambda^{(1)}_{\alpha}(q_n) = \sqrt{\left(\cos q_n + 1\right)^2 + f^2_{\alpha}(q_n)} \tag{1.92}$$

After cutting the whole system into two equal parts (A and B of length $L/2$) we compute the half-chain von Neumann entropy

$$S_{L/2}(t) = -\mathrm{Tr}\,\rho_A(t)\log_2\rho_A(t) \tag{1.93}$$

where A is the reduced density matrix of A, computed by tracing out the B degrees of freedom

$$\rho_A(t) = \mathrm{Tr}_B\,|\psi(t)\rangle\langle\psi(t)| \tag{1.94}$$

In order to get $S_{L/2}(t)$ we need the equal-time correlation matrices $\mathbb{C}_{ij}(t) = \langle c^{\dagger}_i(t)c_j(t)\rangle$ and $\mathbb{F}_{ij} = \langle c^{\dagger}_i(t)c^{\dagger}_j(t)\rangle$, where in the Heisenberg representation operators $c_j(t)$ evolve by $H^{(1)}$

$$c_j(t) = \mathrm{e}^{\mathrm{i}H^{(1)}t}c_j\mathrm{e}^{-\mathrm{i}H^{(1)}t} \tag{1.95}$$

and expectation values are computed over $|\psi^{(0)}\rangle$.

Correlation functions are

$$\begin{aligned}\langle c^{\dagger}_i(t)c^{\dagger}_j(t)\rangle = \frac{1}{L}\sum_{n}^{L/2-1} \sin\left(q_n(i-j)\right)\Big[&\sin 2\theta^{(1)}_{q_n}\cos\left(2\theta^{(0)}_{q_n} - 2\theta^{(1)}_{q_n}\right)\\ &+ \sin\left(2\theta^{(0)}_{q_n} - 2\theta^{(1)}_{q_n}\right)\Big[\cos^2\theta^{(1)}_{q_n}\mathrm{e}^{2\mathrm{i}t\lambda^{(1)}_{\alpha}(q_n)}\\ &- \sin^2\theta^{(1)}_{q_n}\mathrm{e}^{-2\mathrm{i}t\lambda^{(1)}_{\alpha}(q_n)}\Big]\Big]\end{aligned} \tag{1.96}$$

and

$$\begin{aligned}\langle c^{\dagger}_i(t)c_j(t)\rangle = \frac{2}{L}\sum_{n}^{L/2-1} \cos\left(q_n(i-j)\right)\Big[&\sin^2\left(2\theta^{(1)}_{q_n} - \theta^{(0)}_{q_n}\right)\sin^2(\lambda^{(1)}_{\alpha}(q_n)t)\\ &+ \sin^2\theta^{(0)}_{q_n}\cos^2(\lambda^{(1)}_{\alpha}(q_n)t)\Big].\end{aligned} \tag{1.97}$$

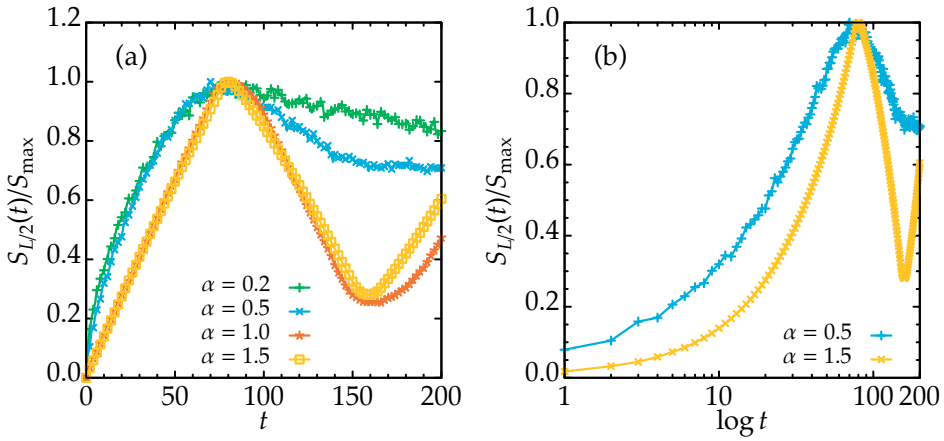

Figure 1.9: The plots show the evolution of the entanglement entropy in a system of $L = 400$ sites after a quench from a product state with $\mu_0 \gg 1$ to $\mu_1 = 1$. For $\alpha > 1$, $S_{L/2}(t)$ grows linearly. For $\alpha < 1$, $S_{L/2}(t)$ grows logarithmically. Panel (a) linear-linear plot. For $\alpha < 1$ $S_{L/2}(t)$ deviates from a straight line. Panel (b) linear-log plot of $S_{L/2}(t)$. The logarithmic behaviors is visible for intermediate time $10 < t < 100$

and the technique to compute $S_{L/2}(t)$ from them is explained in section 1.B.1.

Plots in Figure 1.9 show the different behavior of the entropy in time for different values of α after a quench from $\mu_0 = 1000$.

If $\alpha > 1$ we have a linear growth, as predicted for a conformal field theory by eq. (1.89). If $\alpha \lesssim 1$ the entropy scales logarithmically in time.

In panel (b) of Figure 1.9 we plot $S_{L/2}(t)/S_{\max}$ where $S_{\max}$ is the maximum of the entropy before it starts to oscillate. The oscillations (most visible for $\alpha > 1$) are peculiar to a finite length system for which we used summations for evaluated the correlation functions in (1.96) and (1.97).

If instead we let $L \to \infty$ and replace summation with integrals in (1.96) and (1.97), the oscillations disappear as one can see in Figure 1.10 showing the plots for various α of the scaling of the entanglement entropy for a block of $\ell = 100$ sites.

As for a conformal field theory we expect a linear behavior in time of the entanglment entropy, its logarithmic scaling can be considered as a proof of the breaking of the conformal invariance of the model when $\alpha \lesssim 1$.

1.6 Majorana edge states

The existence of Majorana fermions, (particles that are their own antiparticles) was predicted by Majorana [88] in 1937.

Apart from the theoretical interest Majorana fermions display, they have been proposed as model to engineering one-dimensional quantum states

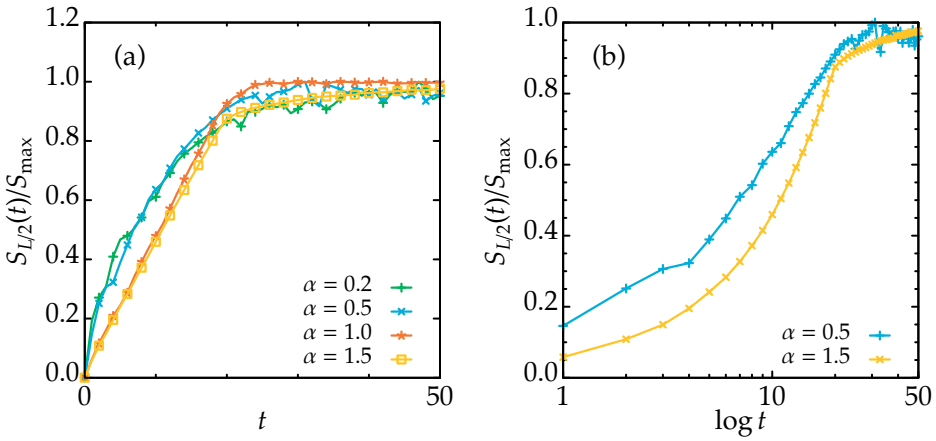

Figure 1.10: The plot shows the scaling of the entanglement entropy in time for a block of $\ell = 100$ sites embedded in a infinite long system. For $\alpha \lesssim 1$ the entropy scales as a logarithm, while for $\alpha > 1$ the entropy grows linearly.

strongly protected against decoherence and suitable to build e.g. quantum memories.

Robustness against decoherence is guaranteed if these states are well separated from the rest of the spectrum of excitations. A first proposal to construct them in a condensed matter system was given by Kitaev in [29].

In this section we discuss how Majorana edge states, already found in the short range limit $\alpha \to \infty$ of Hamiltonian (1.6), appear also in the long-range model.

In limit $\alpha \to \infty$ (and with open boundary conditions), the resulting Hamiltonian is:

$$\begin{aligned} H(\alpha \to \infty) = -w \sum_{j=1}^{L-1} \left(c_j^\dagger c_{j+1} + c_{j+1}^\dagger c_j \right) - \mu \sum_{j=1}^{L} \left(c_j^\dagger c_j - \frac{1}{2} \right) \\ + \Delta \sum_{j=1}^{L-1} \left(c_j c_{j+1} + c_{j+1}^\dagger c_j^\dagger \right) \end{aligned} \tag{1.98}$$

We can decompose each of the c_j Dirac fermions into two Majorana fermions

$$c_j^\dagger = a_j + \mathrm{i} b_j \qquad c_j = a_j - \mathrm{i} b_j \tag{1.99}$$

that are hermitian and satisfy

$$\{a_i, a_j\} = \{b_i, b_j\} = 2\delta_{i,j} \qquad \{a_i, b_j\} = 0 \tag{1.100}$$

$$a_i^2 = b_i^2 = \mathbb{1} \tag{1.101}$$

and we can rewrite $H(\alpha \to \infty)$ as (we will set $\Delta = w$)

$$H(\alpha \to \infty) = 2\mathrm{i} w \sum_{j=1}^{L-1} a_j b_{j+1} - \mathrm{i} \mu \sum_{j=1}^{L} b_j a_j \tag{1.102}$$

Such Hamiltonian, as well as Hamiltonian (1.6), does not conserve the fermion number generated by $F = \sum_{j=1}^{L} c_j^\dagger c_j$ but only parity $\mathscr{P}$ of the fermion number, given by

$$\mathscr{P} = (-1)^F = \prod_{i=1}^{L} (-\mathrm{i} a_i b_i) \tag{1.103}$$

and generating a $\mathscr{Z}_2$ symmetry.

In this way, Hamiltonian is decomposed into two sectors with even or odd fermionic number.

Following [89], we can now define a fermionic zero-energy mode as an operator Ψ that

(i) commutes with the Hamiltonian: $[H, \Psi] = 0$;

(ii) anticommutes with $\mathscr{P}$: $\{\mathscr{P}, \Psi\} = 0$;

(iii) can be normalized even in the $L \to \infty$ limit: $\Psi^\dagger \Psi = 1$.

We can now show that Hamiltonian (1.102) supports zero edge modes by constructing Ψ explicitly.

Commuting $H(\alpha \to \infty)$ with b_1 gives $2\mathrm{i}\mu a_1$. Now, we can rewrite $2a_1 = [a_1 b_2, b_2]$ and the following combination of a_1 and a_2 commutes with the two terms of $H(\alpha \to \infty)$:

$$\left[\mathrm{i}\mu a_1 b_1 + 2w\mathrm{i} a_1 b_2, b_1 - \frac{\mu}{2w} b_2\right] = 0 \tag{1.104}$$

In this way we can define two operators localized at the edge of the chain Ψ_{left} and Ψ_{right}

$$\Psi_{\text{left}} = b_1 - \frac{\mu}{2w} b_2 + \left(\frac{\mu}{2w}\right)^2 b_3 + \ldots \tag{1.105}$$

and

$$\Psi_{\text{right}} = a_L - \frac{\mu}{2w} a_{L-1} + \left(\frac{\mu}{2w}\right)^2 a_{L-2} + \ldots \tag{1.106}$$

Then, the commutators of Ψ_{left} and Ψ_{right} with the Hamiltonian

$$[H(\alpha \to \infty), \Psi_{\text{left}}] = \mu \left(\frac{\mu}{2w}\right)^{L-1} a_L \tag{1.107}$$

$$\left[H(\alpha \to \infty), \Psi_{\text{right}}\right] = \mu \left(\frac{\mu}{2w}\right)^{L-1} b_1 \tag{1.108}$$

are exponentially suppressed in the limit $L \to \infty$ if $|\mu| < 2w$ and in this region we have the appearance of two Majorana states Ψ_{left} and Ψ_{right} localized at the edges of the chain.

If we now consider the long-range Hamiltonian (1.6) in a closed chain (with $d_\ell = \ell$) and with $\Delta = 2w = 1$ we can numerically diagonalize it using

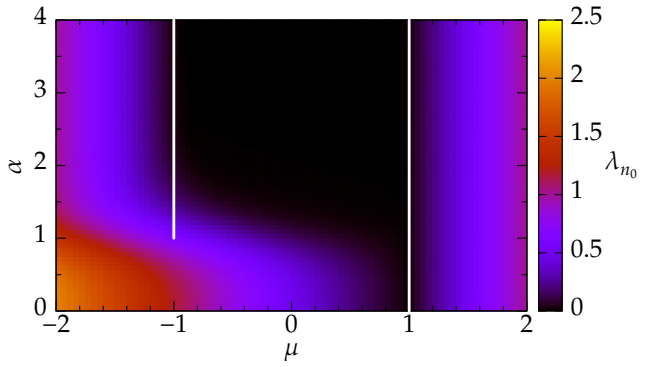

Figure 1.11: The plot shows the minimum among the λ_n of the excitation spectrum of (1.110) for a system of $L = 200$ sites. The white vertical lines are gapless lines. In the black region $|\mu| < 1$, $\alpha \gtrsim 1$ there exists a $\lambda_{n_0} = 0$, that represents a zero mode edge state degenerate with the ground state.

the method reported in [32, 90–92] for finding whether zero energy modes exist.

Given a fermionic quadratic Hamiltonian

$$H = \sum_{i,j=1}^{L} c_i^\dagger \boldsymbol{A}_{ij} c_j + \left(c_i^\dagger \boldsymbol{B}_{ij} c_j^\dagger + \text{h.c.} \right) \tag{1.109}$$

where the matrix $\boldsymbol{A}$ is symmetric and $\boldsymbol{B}$ is antisymmetric, we can cast the Hamiltonian H in diagonal form

$$H = \sum_{n=1}^{L} \lambda_n \eta_n^\dagger \eta_n \tag{1.110}$$

with $\lambda_n \geq 0$ by means of a Bogolyubov transformation

$$\begin{pmatrix} \boldsymbol{\eta} \\ \boldsymbol{\eta}^\dagger \end{pmatrix} = \begin{pmatrix} \boldsymbol{g} & \boldsymbol{h} \\ \boldsymbol{h} & \boldsymbol{g} \end{pmatrix} \begin{pmatrix} \boldsymbol{c} \\ \boldsymbol{c}^\dagger \end{pmatrix} \tag{1.111}$$

where $\boldsymbol{c} = (c_1, \dots, c_L)^T$ the same for $\boldsymbol{\eta}$ and $\boldsymbol{g}$ and $\boldsymbol{h}$ are $L \times L$ matrices.

For getting the single particle energies $\boldsymbol{\lambda} = (\lambda_1, \dots, \lambda_L)^T$ and the matrices $\boldsymbol{g}$ and $\boldsymbol{h}$ we can employ a singular-value decomposition of the sum of $\boldsymbol{A} + \boldsymbol{B}$

$$\boldsymbol{\lambda} = \boldsymbol{\psi}(\boldsymbol{A} + \boldsymbol{B})\boldsymbol{\phi}^T \tag{1.112}$$

where $\boldsymbol{\psi} = \boldsymbol{g} - \boldsymbol{h}$ and $\boldsymbol{\phi} = \boldsymbol{g} + \boldsymbol{h}$.

If a zero energy mode exists we will find the minimum among the single particle energies (we will call it λ_{n_0}) vanishing in a gapped region in the limit $L \to \infty$.

To distinguish it from a zero mode due to a critical point we can look at the exact dispersion relation (1.17) (valid also for open boundary conditions

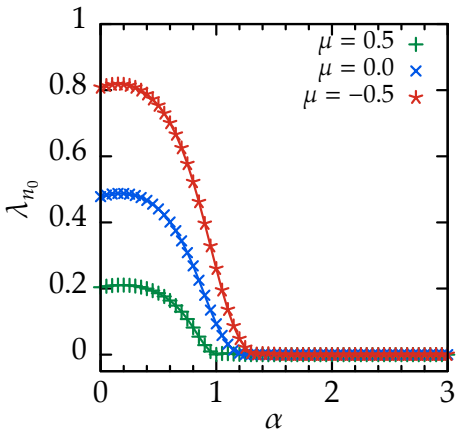

Figure 1.12: Panel (a) shows the value of λ_{n_0} in the limit $L \to \infty$. When $\alpha < 1$, λ_{n_0} becomes finite in the thermodynamic limit and the zero energy mode disappears.

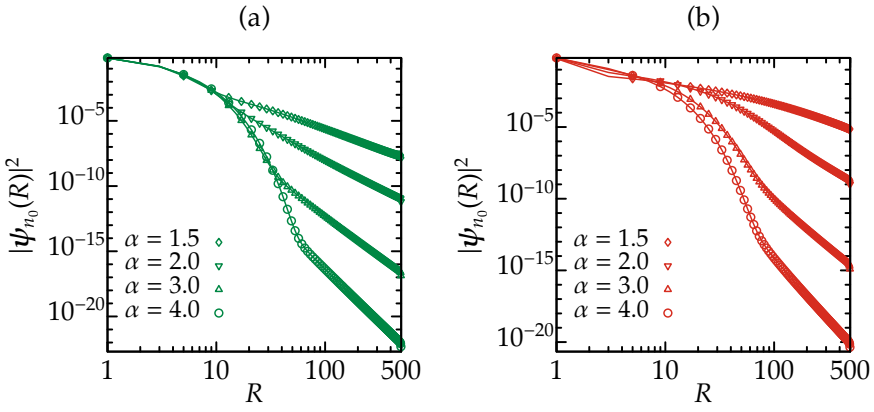

Figure 1.13: The plot shows the wavefunction of the edge mode for a chain of $L = 500$ sites for (a) $\mu = 0.5$ and (b) $\mu = -0.5$ in log-log scale for the different α. It is possible to see the hybrid exponential and power-law behavior (with a tail $1/R^{2\alpha}$) also found for the correlation functions.

as, when $L \to \infty$, the bulk properties are the same both for a ring and for a closed chain). We know that the critical lines are only $\mu = 1, \alpha > 0$ and $\mu = -1, \alpha > 1$ and, thus a $\lambda_{n_0} = 0$ for $\mu \neq \pm 1$ will correspond to a true zero energy mode.

The plot in Figure 1.11 represents the position of these zero energy points where two degenerate ground states appear.

We find that the gapped region $|\mu| < 1$ for $\alpha \gtrsim 1$ supports zero energy modes and we fitted the value of $\lambda_{n_0}(L)$ as function of L for different α and μ. Plot in Figure 1.12 shows the thermodynamical values for λ_{n_0} as function of α for several μ and when $\alpha < 1$ one can see that these modes become massive.

Moreover, we can access to the wavefunction of these zero modes, by plotting the normalized square of the n_0-th row of ψ or ϕ (corresponding to the eigenvalue λ_{n_0}) as function of the lattice site R (Figure 1.13). Remarkably, its wavefunction mirrors the hybrid exponential and power-law decay we discussed for the correlation functions.

By fitting the power-law tail of $|\psi_{n_0}(R)|^2$ we found $|\psi n_0(R)|^2 \sim R^{-2\alpha}$ for $\alpha \gtrsim 1$, implying that $|\psi n_0(R)|^2$ is normalizable, as required for an edge mode.

We also note that this algebraic decay is in qualitative agreement with recent calculations for helical Shiba chains [93].

1.7 Conclusions

In this Chapter, motivated by recent experimental setups for the realization of systems supporting long-range interactions, we have presented and analyzed an integrable model for fermions with long-range pairing, finding several novel features.

These include gapped phases where correlation functions exhibit purely algebraic or hybrid exponential-algebraic decay.

Moreover, we demonstrate a breaking of the conformal symmetry along gapless lines accompanied by a violation of the area law in gapped phases for sufficiently long-range interactions.

It is an exciting prospect to investigate whether some of the results of the present work are in fact common to other models with long-range interactions, such as, e.g., Ising-type models with tunable interactions, as currently realized in several labs [19, 28]. As we have shown that the breaking of conformal symmetry may be directly detected in the dynamics of the von Neumann entropy following a quench, as recently demonstrated numerically for ion chains [39], it would be worth to find an exact expression (like the ones in (1.81) and (1.89)) both for the scaling of the static entropy and its time evolution after a quench in order to integrate the already known results on finite-range interactions [94].

Appendices

1.A XY-Ising model

In this Appendix, I will review some results on the exact diagonalization of the XY model [32].

We consider the following spin hamiltonian with periodic boundary condition on a chain of N (even) sites:

$$H(\gamma, h) = -J \sum_{j=1}^{N} \left[(1+\gamma) S_j^x S_{j+1}^x + (1-\gamma) S_j^y S_{j+1}^y \right] + Jh \sum_{j=1}^{N} S_j^z \tag{1.113}$$

The spin operator are defined in terms of the Pauli matrices:

$$S^x = \frac{1}{2}\begin{pmatrix} 0 & 1 \\ 1 & 0 \end{pmatrix} \quad S^y = \frac{1}{2}\begin{pmatrix} 0 & -\mathrm{i} \\ \mathrm{i} & 0 \end{pmatrix} \quad S^z = \frac{1}{2}\begin{pmatrix} 1 & 0 \\ 0 & -1 \end{pmatrix}$$

and, by employing ladder operators:

$$S_i^+ = S_i^x + \mathrm{i} S_i^y \tag{1.114}$$

$$S_i^- = S_i^x - \mathrm{i} S_i^y \tag{1.115}$$

one can rewrite the spin Hamiltonian as

$$H(\gamma, h) = -J \sum_{j=1}^{N} \left[\frac{1}{2} \left(S_j^+ S_{j+1}^- + S_j^- S_{j+1}^+ \right) + \frac{\gamma}{2} \left(S_j^+ S_{j+1}^+ + S_j^- S_{j+1}^- \right) + Jh S_j^z \right] \tag{1.116}$$

and, after a Jordan-Wigner (JW) transformation

$$S_i^+ = c_i^\dagger \exp\left(\mathrm{i}\pi \sum_{l=1}^{i-1} c_l^\dagger c_l \right) \tag{1.117}$$

$$S_i^- = \exp\left(-\mathrm{i}\pi \sum_{l=1}^{i-1} c_l^\dagger c_l \right) c_i \tag{1.118}$$

$$S_i^z = c_i^\dagger c_i - \frac{1}{2} \tag{1.119}$$

the Hamiltonian becomes:

$$\begin{aligned} H(\gamma,h) = &-\frac{J}{2}\sum_{j=1}^{N-1}\left[c_j^\dagger c_{j+1} - c_j c_{j+1}^\dagger + \gamma\left(c_j^\dagger c_{j+1}^\dagger - c_j c_{j+1}\right)\right] \\ &+ Jh\sum_{j=1}^{N}\left(c_i^\dagger c_i - \frac{1}{2}\right) \\ &+ \frac{J}{2}\mathrm{e}^{\mathrm{i}\pi\sum_{l=1}^{N} c_l^\dagger c_l}\left[c_N^\dagger c_{N+1} - c_N c_{N+1}^\dagger + \gamma\left(c_N^\dagger c_{N+1}^\dagger - c_N c_{N+1}\right)\right] \end{aligned} \tag{1.120}$$

The parity $\mathscr{P} = \exp(\mathrm{i}\pi\sum_{l=1}^{N} c_l^\dagger c_l)$ of the number of fermions commutes with the Hamiltonian, so there exist two sectors of the Hilbert space in which the Hamiltonian and the operator $\mathscr{P}$ can be diagonalized simultaneously.

Since $\mathscr{P}$ is unitary, its eingenvalues can be only +1 or −1, so its spectral decomposition is $\mathscr{P} = P_+ - P_-$ and $H(\gamma,h)$ decomposes as

$$H(\gamma,h) = H^+(\gamma,h) + H^-(\gamma,h) \tag{1.121}$$

with $H^\pm(\gamma,h) = P_\pm H(\gamma,h)P_\pm$

Even fermion number $\mathscr{P} = 1$

We choose the sector with parity $\mathscr{P} = 1$ (with an even number of fermions). In this case we have to choose anti-periodic boundary conditions for the Jordan-Wigner fermions ($c_{N+1} = -c_1$), so, if we perform a Fourier transform, momenta will be:

$$k_n = \frac{2\pi}{N}\left(n + \frac{1}{2}\right) \tag{1.122}$$

and the fermionic operators

$$c_i^\dagger = \frac{1}{\sqrt{N}}\sum_{n=0}^{N-1}\mathrm{e}^{\mathrm{i}k_n x_i}c_n^\dagger. \tag{1.123}$$

The Hamiltonian in the parity +1 sector is:

$$\begin{aligned} H^+(\gamma,h) = -\frac{J}{2}\sum_{n=0}^{N-1}\Big[&(\cos k_n - h)(c_n^\dagger c_n + c_{-n-1}^\dagger c_{-n-1}) \\ &+\mathrm{i}\gamma\sin k_n(c_{-n-1}^\dagger c_n^\dagger + c_{-n-1}c_n)\Big] - \frac{JhN}{2} \end{aligned} \tag{1.124}$$

Note that the term $\sin k_n$ is always different from zero, due to the antiperiodic boundary conditions for the JW fermions and the even number of site N.

We can introduce a spinor $\begin{pmatrix} c_n^\dagger & c_{-n-1}\end{pmatrix}$ and the Hamiltonian takes the form

$$H^+(\gamma,h) = \frac{J}{2}\sum_n \begin{pmatrix} c_n^\dagger & c_{-n-1}\end{pmatrix}\begin{pmatrix} -(\cos k_n - h) & \mathrm{i}\gamma\sin k_n \\ -\mathrm{i}\gamma\sin k_n & (\cos k_n - h)\end{pmatrix}\begin{pmatrix} c_n \\ c_{-n-1}^\dagger\end{pmatrix} \tag{1.125}$$

and, after a Bogolyubov transformation

$$\begin{pmatrix} c_n \\ c^\dagger_{-n-1} \end{pmatrix} = U^\dagger \begin{pmatrix} \eta_n \\ \eta^\dagger_{-n-1} \end{pmatrix} \tag{1.126}$$

with

$$U = \begin{pmatrix} \alpha_n & -\beta^*_n \\ \beta_n & \alpha^*_n \end{pmatrix} = \begin{pmatrix} \cos\theta_n & \mathrm{i}\sin\theta_n \\ \mathrm{i}\sin\theta_n & \cos\theta_n \end{pmatrix} \tag{1.127}$$

and

$$\tan 2\theta_n = \frac{\gamma \sin k_n}{h - \cos k_n} \tag{1.128}$$

the Hamiltonian becomes:

$$H^+(\gamma, h) = \sum_{n=0}^{N-1} \lambda(k_n) \left(\eta^\dagger_n \eta_n - \frac{1}{2} \right) \tag{1.129}$$

with

$$\lambda(k_n) = J\sqrt{(\cos k_n - h)^2 + \gamma^2 \sin^2 k_n} \tag{1.130}$$

The ground state of $H^+(\gamma, h)$ is the vacuum of η_n: $\eta_n |GS_{\gamma,h}\rangle = 0$. A possible choice for this state is

$$|GS_{\gamma,h}\rangle^+ = \prod_{n=0}^{N-1} \eta_n \eta_{-n-1} |0\rangle = \prod_{n=0}^{\frac{N}{2}-1} (\alpha_n + \beta^*_n c^\dagger_n c^\dagger_{-n-1}) |0\rangle \tag{1.131}$$

and its energy density is

$$E^+_0(\gamma, h) = -\frac{1}{2} \sum_{n=0}^{N-1} \lambda(k_n) \tag{1.132}$$

To compute the actual ground state of the XY model we need to look also at the spectrum of the $H^-(\gamma, h)$ Hamiltonian.

Odd fermion number $\mathscr{P} = -1$

In this case JW fermions are periodic so, momenta will be

$$k_n = \frac{2\pi n}{N} \tag{1.133}$$

and the Hamiltonian is

$$H^-(\gamma, h) = \frac{J}{2} \sum_{n=0}^{N-1} \begin{pmatrix} c^\dagger_n & c_{-n} \end{pmatrix} \begin{pmatrix} -(\cos k_n - h) & \mathrm{i}\gamma \sin k_n \\ -\mathrm{i}\gamma \sin k_n & (\cos k_n - h) \end{pmatrix} \begin{pmatrix} c_n \\ c^\dagger_{-n} \end{pmatrix} \tag{1.134}$$

The term with $\sin k_n = 0$ needs to be kept apart from the others

$$\begin{aligned} H^{-}(\gamma,h) = &-J(1-h)\left(c_0^\dagger c_0 - \frac{1}{2}\right) \\ &+ \frac{J}{2}\sum_{n=1}^{N-1}\begin{pmatrix} c_n^\dagger & c_{-n}\end{pmatrix}\begin{pmatrix} -(\cos k_n - h) & \mathrm{i}\gamma \sin k_n \\ -\mathrm{i}\gamma \sin k_n & (\cos k_n - h)\end{pmatrix}\begin{pmatrix} c_n \\ c_{-n}^\dagger\end{pmatrix} \end{aligned} \tag{1.135}$$

Now we have to deal with the two cases $h > 1$ and $h < 1$ separately.

$h < 1$

If $h < 1$ the Hamiltonian is

$$\begin{aligned} H^{-}(\gamma,h) = &-J|1-h|\left(c_0^\dagger c_0 - \frac{1}{2}\right) \\ &+ \frac{J}{2}\sum_{n=1}^{N-1}\begin{pmatrix} c_n^\dagger & c_{-n}\end{pmatrix}\begin{pmatrix} -(\cos k_n - h) & \mathrm{i}\gamma \sin k_n \\ -\mathrm{i}\gamma \sin k_n & (\cos k_n - h)\end{pmatrix}\begin{pmatrix} c_n \\ c_{-n}^\dagger\end{pmatrix} \end{aligned} \tag{1.136}$$

Since the first term decreases the energy of the ground state, we employ a particle-hole transformation for the $\left(c_0^\dagger, c_0\right)$ and a Bogolyubov transformation for the $\left(c_n^\dagger, c_n\right)$ with $n > 0$:

$$\xi_0 = c_0^\dagger \tag{1.137}$$
$$\xi_0^\dagger = c_0 \tag{1.138}$$
$$\xi_n = \alpha_n c_n - \beta_n^* c_{-n}^\dagger \tag{1.139}$$
$$\xi_{-n}^\dagger = \beta_n c_n + \alpha_n^* c_{-n}^\dagger \tag{1.140}$$

which yield to

$$H^{-}(\gamma, h<1) = J|h-1|\left(\xi_0^\dagger\xi_0 - \frac{1}{2}\right) + \sum_{n=1}^{N-1}\lambda(k_n)\left(\xi_n^\dagger\xi_n - \frac{1}{2}\right) \tag{1.141}$$

The ground state in this case is

$$|GS_{\gamma,h<1}\rangle^{-} = \xi_0\prod_{n=1}^{N-1}\xi_n\xi_{-n}\,|0\rangle = c_0^\dagger\prod_{n=1}^{\frac{N}{2}}(\alpha_n + \beta_n^* c_n^\dagger c_{-n}^\dagger)\,|0\rangle \tag{1.142}$$

and its energy

$$E_0^{-}(\gamma, h<1) = -\frac{J}{2}|h-1| - \sum_{n=1}^{N-1}\lambda(k_n) \tag{1.143}$$

The operator ξ_0 is needed because $|GS_{\gamma,h<1}\rangle^{-}$ must belong to the sector with an odd number of fermions.

$h > 1$

If $h > 1$ the Hamiltonian is

$$\begin{aligned} H^{-}(\gamma, h) = J|h-1|\left(c_0^\dagger c_0 - \frac{1}{2}\right) \\ + \frac{J}{2}\sum_{n=1}^{N-1}\begin{pmatrix} c_n^\dagger & c_{-n}\end{pmatrix}\begin{pmatrix} -(\cos k_n - h) & \mathrm{i}\gamma \sin k_n \\ -\mathrm{i}\gamma \sin k_n & (\cos k_n - h)\end{pmatrix}\begin{pmatrix} c_n \\ c_{-n}^\dagger\end{pmatrix} \end{aligned} \tag{1.144}$$

In this case $\lambda(k_n) = J\sqrt{(\cos k_n - h)^2 + \gamma^2 \sin^2 k_n}$ implies that $\lambda(k_0) = J|h-1|$ so by means of the following unitary transformation

$$\psi_0 = c_0 \tag{1.145}$$
$$\psi_0^\dagger = c_0^\dagger \tag{1.146}$$
$$\psi_n = \alpha_n c_n - \beta_n^* c_{-n}^\dagger \tag{1.147}$$
$$\psi_{-n}^\dagger = \beta_n c_n + \alpha_n^* c_{-n}^\dagger \tag{1.148}$$

the Hamiltonian takes the form:

$$H^{-}(\gamma, h > 1) = \sum_{n=0}^{N-1}\lambda(k_n)\left(\psi_n^\dagger \psi_n - \frac{1}{2}\right) \tag{1.149}$$

The ground state in this case is

$$|GS_{\gamma,h>1}\rangle^{-} = c_0^\dagger \prod_{n=1}^{\frac{N}{2}}(\alpha_n + \beta_n^* c_n^\dagger c_{-n}^\dagger)\,|0\rangle \tag{1.150}$$

and its energy

$$E_0^{-}(\gamma, h > 1) = \lambda(k_0) - \sum_{n=0}^{N-1}\lambda(k_n) = J|h-1| - \frac{1}{2}\sum_{n=0}^{N-1}\lambda(k_n) \tag{1.151}$$

Ground state of the XY model

We can now construct the ground state of the model at finite number of sites.

We consider first the section $h > 1$. In this case, $E_0^{-}(\gamma, h > 1)$ is always larger than $E_0^{+}(\gamma, h)$ so the ground state, for all γ and h belongs to the sector with an even number of fermions and it is $|GS_{\gamma,h}\rangle^{+}$.

In the range $h < 1$ the ground state is either $|GS_{\gamma,h}\rangle^{+}$ or $|GS_{\gamma,h<1}\rangle^{-}$ depending on whether $E_0^{+}(\gamma, h)$ is smaller or larger than $E_0^{-}(\gamma, h < 1)$, however if one considers the Ising model, given by $\gamma = 1$, one can show that the ground state, in the region $h < 1$ is still given by $|GS_{1,h}\rangle^{+}$.

Finite size scaling of the ground-state energy

Finite size scaling of the ground state energy density can give insights on the conformal field theory underlying a critical point.

In particular, it is known that the ground state energy density $e(L)$ of a critical conformal model in a system of dimension L scales as

$$e(L) = e^{\infty} - \frac{\pi c v_F}{6L^2} \tag{1.152}$$

where e^{∞} is the bulk energy and v_F is the Fermi velocity at the critical momentum, that is the slope of the dispersion relation when it vanishes.

In the following section we will compute the exact scaling for the ground state energy density of the XY-Ising model, given by (we will consider the antiperiodic sector where $k_n = 2\pi(n + 1/2)/L$)

$$e(L) = -\frac{1}{L}\sum_{n=0}^{L/2-1} \lambda(k_n). \tag{1.153}$$

For evaluating the sum we will use the Euler-MacLaurin summation formula [95].

Let $f(x)$ have its first two derivatives continuous on an interval (a, b). If we divide the interval in n parts and let $\delta = (b - a)/n$, then

$$\begin{aligned}\sum_{j=0}^{n} f(a + j\delta) = \frac{1}{\delta}\int_a^b f(x)\mathrm{d}x + \frac{1}{2}\Big(f(b) + f(a)\Big) \\ + \frac{\delta}{12}\Big(f'(b) - f'(a)\Big)\end{aligned} \tag{1.154}$$

In our case $a = \pi/L$, $\delta = 2\pi/L$, $n = L/2 - 1$ and the expansion of the previous equation up to $\mathscr{O}(1/L^2)$ gives

$$\sum_{j=0}^{n} f\left(k_n\right) = \frac{L}{2\pi}\int_0^{\pi} f(x)\,\mathrm{d}x + \frac{\pi}{12L}\Big(f'(0) - f'(\pi)\Big) \tag{1.155}$$

If the ground state energy density is given by

$$e(L) = -\frac{1}{L}\sum_{n=0}^{L/2-1} \lambda(k_n) \tag{1.156}$$

we have

$$e(L) = -\frac{1}{2\pi}\int_0^{\pi} \lambda(x)\,\mathrm{d}x - \frac{\pi}{12L^2}\left(\lambda'(0) - \lambda'(\pi)\right). \tag{1.157}$$

Let us apply the previous equation to the XY-Ising model for which

$$\lambda(k) = \sqrt{(\cos k - h)^2 + \gamma^2 \sin^2 k}. \tag{1.158}$$

We have seen that it shows a phase transition for a critical field $h_c = 1$, corresponding to a critical momentum $k_c = 0$. The Fermi velocity is thus given by

$$v_F = \frac{\mathrm{d}}{\mathrm{d}k}\lambda(k)\Big|_{k=0} = \gamma \tag{1.159}$$

and the finite-size correction is

$$e(L) = -\frac{1}{2\pi}\int_0^\pi \lambda(x)\,\mathrm{d}x - \frac{\pi\gamma}{12L^2} \tag{1.160}$$

giving $c = 1/2$ as expected.

1.B Density matrix from correlation functions

In this Appendix we will review of the method to compute the ground-state density matrix for a free fermionic Hamiltonian. If the Hamiltonian of the system is quadratic, it is always possible to cast it in the following form

$$H = \sum c_i^\dagger t_{ij} c_j + \left(c_i^\dagger U_{ij} c_j^\dagger + \text{h.c.}\right). \tag{1.161}$$

Let the ground state of (1.161) be $|GS\rangle$ with its density matrix $|GS\rangle\langle GS|$.

Let us divide the systems into two intervals (A and B) with the first ℓ sites belonging to A, the others to B.

We want to compute the reduced density matrix $\rho_A = \mathrm{Tr}_B\,|GS\rangle\langle GS|$ of the ground state related to the subsystem A, by tracing out the degrees of freedom of B.

To this end, we note that to reproduce the expectation value in the ground state of a string of fermionic operators all belonging to A, the density matrix has to be [49, 96–100]

$$\rho_A = \frac{\mathrm{e}^{-\mathscr{H}}}{Z} \tag{1.162}$$

with

$$\mathscr{H} = \sum_{i,j=1}^{\ell} c_i^\dagger A_{ij} c_j + \left(c_i^\dagger B_{ij} c_j^\dagger + \text{h.c.}\right). \tag{1.163}$$

having the same functional form as (1.161).

This means that all the information on ρ_A is encoded in the correlator matrices

$$\mathbb{C}_{ij} = \langle c_i^\dagger c_j\rangle \qquad \mathbb{F}_{ij} = \langle c_i^\dagger c_j^\dagger\rangle \tag{1.164}$$

with $1 \le i,j \le \ell$.

$\mathbb{C}$ and $\mathbb{F}$ are easily computed from the ground state of the Hamiltonian (1.161), as the latter is readily diagonalized with a Bogolyubov transformation or following [32, 92].

Then, one can relate the correlation matrices with the eigenvalues of the entanglement Hamiltonian $\mathscr{H}$ (1.163) and so with the density matrix ρ.

To compute those matrices, we first diagonalize (1.163) with a Bogolyubov transformation:

$$\begin{pmatrix} \eta \\ \eta^\dagger \end{pmatrix} = \begin{pmatrix} g & h \\ h & g \end{pmatrix} \begin{pmatrix} c \\ c^\dagger \end{pmatrix} \tag{1.165}$$

where g and h are $\ell \times \ell$ real matrices, satisfying, because of the anticommutation relations:

$$gg^T + hh^T = \mathbb{1} \tag{1.166}$$
$$gh^T + hg^T = \mathbb{0} \tag{1.167}$$

where g^T is the transpose of the matrix g.

In this basis, $\mathscr{H}$ takes the form

$$\mathscr{H} = \sum_{k=1}^{\ell} \varepsilon_k \eta_k^\dagger \eta_k \tag{1.168}$$

and the density matrix $\rho = \otimes \rho_k$, with :

$$\rho_k = \frac{\mathrm{e}^{-\varepsilon_k \eta_k^\dagger \eta_k}}{1 + \mathrm{e}^{-\varepsilon_k}} = \begin{pmatrix} (1+\mathrm{e}^{\varepsilon_k})^{-1} & 0 \\ 0 & (1+\mathrm{e}^{-\varepsilon_k})^{-1} \end{pmatrix} \tag{1.169}$$

as each of the ℓ modes is independent.

Now to compute the correlation matrices, we have to find the inverse of the Bogolyubov transformation:

$$\begin{pmatrix} c \\ c^\dagger \end{pmatrix} = \begin{pmatrix} g^T & h^T \\ h^T & g^T \end{pmatrix} \begin{pmatrix} \eta \\ \eta^\dagger \end{pmatrix} \tag{1.170}$$

and we have to note that

$$\langle \eta_k^\dagger \eta_{k'} \rangle = \mathrm{Tr}\left[\rho\, \eta_k^\dagger \eta_{k'}\right] = \frac{\mathrm{e}^{-\varepsilon_k}}{1+\mathrm{e}^{\varepsilon_k}} \delta_{kk'} \tag{1.171}$$

Let $\mathbb{C}$ be the matrix of the correlators $\langle c_i^\dagger c_j \rangle$ and $\mathbb{F}$ the matrix $\langle c_i^\dagger c_j^\dagger \rangle$ related to the block $1 < i, j < \ell$. We have

$$\mathbb{C} = g^T \Lambda g + h^T \bar{\Lambda} h \tag{1.172}$$
$$\mathbb{F} = g^T \Lambda h + h^T \bar{\Lambda} h \tag{1.173}$$

where $\Lambda, \bar{\Lambda}$ are diagonal matrices with elements

$$\Lambda_{ij} = \frac{\delta_{ij}}{1+\mathrm{e}^{\varepsilon_i}} \qquad \bar{\Lambda}_{ij} = \frac{\delta_{ij}}{1+\mathrm{e}^{-\varepsilon_i}} \tag{1.174}$$

Note that $\Lambda + \bar{\Lambda} = \mathbb{1}$. Let us define $\Delta = \Lambda - \bar{\Lambda}$, so, by using (1.166) we can write the correlators as

$$\mathbb{C} = \frac{\mathbb{1}}{2} + \frac{1}{2}\left(g^T \Delta g - h^T \Delta h\right) \tag{1.175}$$

$$\mathbb{F} = \frac{1}{2}\left(g^T \Delta h - h^T \Delta g\right) \tag{1.176}$$

Now, from the anticommutation relations (1.166), one has (note that $\Delta_{ij} = -\tanh(\varepsilon_i/2)\,\delta_{ij}$)

$$W \equiv \left(C - \frac{\mathbb{1}}{2} + F\right)\left(C - \frac{\mathbb{1}}{2} - F\right) = \frac{1}{4}\left(g - h\right)^T \Delta^2 \left(g - h\right) \tag{1.177}$$

By defining a matrix $\psi = g - h$ one has $\psi^T \psi = \mathbb{1}$ so ψ is orthogonal and, from the previous equation one has

$$W = \frac{1}{4}\psi^T \Delta^2 \psi \tag{1.178}$$

that is the eigenvalues of W are $\zeta_i = \frac{1}{4}\tanh^2(\frac{\varepsilon_i}{2})$. From these one gets the eigenvalues of $\mathscr{H}$:

$$\varepsilon_i = 2\,\mathrm{arctanh}\left(2\sqrt{\zeta_i}\right). \tag{1.179}$$

Once obtained the entanglement spectrum ε_i, the von Neumann entropy, defined as

$$S_{\mathrm{vN}} = -\mathrm{Tr}\,\rho \log_2 \rho = -\sum_{m=1}^{\ell} \mathrm{Tr}\,\rho_m \log_2 \rho_m \tag{1.180}$$

with

$$\rho_m \log_2 \rho_m = \begin{pmatrix} \frac{1}{1+\mathrm{e}^{\varepsilon_m}} \log_2 \frac{1}{1+\mathrm{e}^{\varepsilon_m}} & 0 \\ 0 & \frac{1}{1+\mathrm{e}^{-\varepsilon_m}} \log_2 \frac{1}{1+\mathrm{e}^{-\varepsilon_m}} \end{pmatrix}. \tag{1.181}$$

takes the form

$$S_{\mathrm{vN}} = -\sum_{m=1}^{\ell} \left[\frac{\log_2(1+\mathrm{e}^{\varepsilon_m})}{1+\mathrm{e}^{\varepsilon_m}} + \frac{\log_2(1+\mathrm{e}^{-\varepsilon_m})}{1+\mathrm{e}^{-\varepsilon_m}} \right] \tag{1.182}$$

while the Rényi entropy of order n

$$S_n^{\mathrm{Re}} = \frac{1}{1-n} \log_2 \mathrm{Tr}\,\rho^n \tag{1.183}$$

is

$$S_n^{\mathrm{Re}} = \frac{1}{1-n} \sum_{m=1}^{\ell} \log_2 \left[(1+\mathrm{e}^{\varepsilon_m})^{-n} + (1+\mathrm{e}^{-\varepsilon_m})^{-n}\right] \tag{1.184}$$

1.B.1 *Reduced density matrix after a quench*

In the previous section we have considered only a time-independent situation. Let us consider the dynamical evolution of a state $|\psi\rangle$ by means of a given Hamiltonian H_1, with the assumption that $|\psi\rangle$ is not eigenstate of H.

We will have that the state $|\psi\rangle$ evolves in time as $|\psi(t)\rangle = \mathrm{e}^{-\mathrm{i}H_1 t}|\psi\rangle$ as well as the total $|\psi(t)\rangle\langle\psi(t)|$ and the reduced density matrices.

If H_1 is still quadratic, the arguments of the previous section can be still used to compute the reduced density matrix and the entropy, because, if the initial state is a Slater determinant a string of correlators factor again, because Wick's theorem still holds.

Therefore the reduced density matrix has the exponential form (1.162) with a time-dependent operator $\mathscr{H}(t)$ and the eigenvalues of the entanglement spectrum follow from the equal-time correlation matrices

$$\mathbb{C}_{ij}(t) = \langle c_i^\dagger(t) c_j(t)\rangle \qquad \mathbb{F}_{ij}(t) = \langle c_i^\dagger(t) c_j^\dagger(t)\rangle\,. \tag{1.185}$$

In this case, as $\mathbb{F}$ matrix is, in general, complex, using Majorana fermions defined by

$$a_{2j-1} = c_j + c_j^\dagger \qquad a_{2j} = \mathrm{i}(c_j - c_j^\dagger) \tag{1.186}$$

turns out to be more convenient. Then, in the same way as for the static case, one has to diagonalize the unique $2\ell \times 2\ell$ correlation matrix $\widetilde{\mathbb{C}}_{ij}(t) = \langle a_i(t) a_j(t)\rangle$ whose eigenvalues $m_j(t)$ are related to the entanglement spectrum $\varepsilon_j(t)$ via

$$m_j(t) = 1 \pm \mathrm{i}\tanh\frac{\varepsilon_j(t)}{2}. \tag{1.187}$$

1.C Polylogarithm

The series defining $f_\alpha(k)$ is

$$f_\alpha(k) = \sum_{\ell=1}^{L-1} \frac{\sin(k\ell)}{d_\ell^\alpha} \tag{1.188}$$

with $d_\ell = \min[\ell, L-\ell]$ and, in the thermodynamic limit $L \to \infty$

$$f_\alpha^\infty(k) = \frac{1}{\mathrm{i}} \sum_{\ell=1}^{\infty} \frac{\mathrm{e}^{\mathrm{i}\ell k} + \mathrm{e}^{-\mathrm{i}\ell k}}{\ell^\alpha} = -\mathrm{i}(\mathrm{Li}_\alpha(\mathrm{e}^{\mathrm{i}k}) - \mathrm{Li}_\alpha(\mathrm{e}^{-\mathrm{i}k})) \tag{1.189}$$

where

$$\mathrm{Li}_\alpha(z) = \sum_{\ell=1}^{\infty} \frac{z^\ell}{\ell^\alpha} \tag{1.190}$$

is the polylogarithm of complex z of order α [46, 95]. If $|z| < 1$, the previous series defines an analytic function of z. In our case $z = \mathrm{e}^{\mathrm{i}k}$ so $|z| = 1$ and the

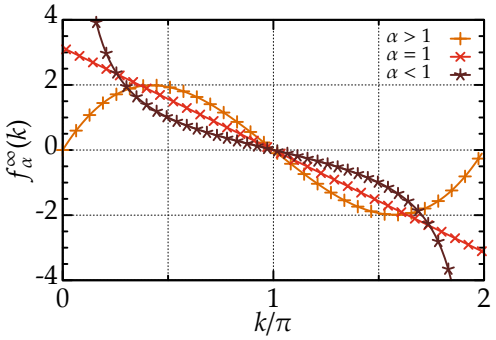

Figure 1.C.1: The plot shows $f_\alpha^\infty(k)$ for $\alpha > 1$, $\alpha = 1$, $\alpha < 1$. If $\alpha < 1$, $f_\alpha^\infty(k)$ diverges if $k \to 0$ as $1/k^{1-\alpha}$.

series converges when $\alpha > 1$. When $\alpha < 1$ the series converges to a finite value for $z \neq 1$ (*i.e.* $k \neq 0$) and diverges as

$$\mathrm{Li}_\alpha(e^{ik}) \sim \Gamma(1-\alpha)\frac{i^\alpha}{k^{1-\alpha}} \quad \text{when } k \to 0. \tag{1.191}$$

In the particular cases of $\alpha = 1$ and $\alpha = 0$ one can get a closed expression for $\mathrm{Li}_\alpha(z)$:

$$\mathrm{Li}_1(z) = -\ln(1-z) \qquad \mathrm{Li}_0(z) = \frac{z}{1-z} \tag{1.192}$$

and for $f_\alpha^\infty(k)$

$$f_1^\infty(k) = \pi - k \qquad f_0^\infty(k) = \cot\left(\frac{k}{2}\right). \tag{1.193}$$

Zeroes

By substituting $k = \pi$ in the last equation of (1.189) one has $f_\alpha^\infty(\pi) = 0$ as $\mathrm{Li}_\alpha(-1)$ (the Dirichlet eta function) is finite for all $\alpha > 0$. The situation is different when $k = 0$. As we said the series converges when $\alpha > 1$, it is finite when $\alpha = 1$, diverges if $\alpha < 1$, so $f_\alpha^\infty(0) = 0$ only when $\alpha > 1$ (see Figure 1.C.1).

Series expansion

The following series expansions were useful for computing the long-distance behavior of correlation functions:

$$\mathrm{Li}_\alpha(e^y) = -\Gamma(1-\alpha)e^{i\pi\alpha}y^{\alpha-1} + \sum_{j=0}^{\infty}\frac{\zeta(\alpha-j)}{j!}y^j, \tag{1.194}$$

$$\mathrm{Li}_\alpha(e^{-y}) = \Gamma(1-\alpha)y^{\alpha-1} + \sum_{j=0}^{\infty}\frac{\zeta(\alpha-j)}{j!}(-y)^j \tag{1.195}$$

for $y \to 0$ and when $\alpha \neq 1, 2, \dots$.

Decay exponent of correlators for integer α

In the following section, we will show how to compute the decay exponent for the Green function (1.39) when α is integer.

If $\alpha \in$ the following series expansions hold ($y \to 0$):

$$\mathrm{Li}_\alpha(\mathrm{e}^y) = \frac{y^{\alpha-1}}{(\alpha-1)!}(H_{\alpha-1} - \ln y - \pi\mathrm{i}) + \sum_{\substack{k=0 \\ k\neq\alpha-1}}^{\infty} \frac{\zeta(\alpha-k)}{k!} y^k \tag{1.196}$$

$$\mathrm{Li}_\alpha(\mathrm{e}^{-y}) = \frac{(-1)^{\alpha-1}y^{\alpha-1}}{(\alpha-1)!}(H_{\alpha-1} - \ln y) + \sum_{\substack{k=0 \\ k\neq\alpha-1}}^{\infty} \frac{\zeta(\alpha-k)}{k!} y^k. \tag{1.197}$$

where H_n is the n-th harmonic number. So,

$$\begin{aligned}\mathrm{Li}_\alpha(\mathrm{e}^y) - \mathrm{Li}_\alpha(\mathrm{e}^{-y}) = \frac{y^{\alpha-1}}{(\alpha-1)!}\left[(1+(-1)^\alpha)H_{\alpha-1} - (1+(-1)^\alpha)\ln y - \pi\mathrm{i}\right] \\ + 2\sum_{\substack{k \text{ odd} \\ k\neq\alpha-1}} \frac{\zeta(\alpha-k)}{k!} y^k\end{aligned}$$

If α is an odd integer, the previous equation reduces to

$$\mathrm{Li}_\alpha(\mathrm{e}^y) - \mathrm{Li}_\alpha(\mathrm{e}^{-y}) = -\frac{\pi\mathrm{i}y^{\alpha-1}}{(\alpha-1)!} + 2\sum_{k \text{ odd}} \frac{\zeta(\alpha-k)}{k!} y^k \tag{1.198}$$

and, recalling eq. (1.55), the leading term of the imaginary part of $\mathscr{G}_\alpha(\mathrm{i}y)$ is

$$\mathrm{Im}\,\mathscr{G}_\alpha(y \to 0) \sim -\frac{\pi\zeta(\alpha-1)}{(\alpha-1)!\,\mathrm{sgn}(1+\mu)(1+\mu)^2} y^\alpha. \tag{1.199}$$

From eq. (1.52) we can compute the long-range contribution to the correlation function:

$$I_{\mathscr{C}_0} + I_{\mathscr{C}_{2\pi}} = -\frac{\alpha\zeta(\alpha-1)}{\mathrm{sgn}\,(\mu+1)(1+\mu)^2} \frac{1}{R^{\alpha+1}}. \tag{1.200}$$

If $\alpha = 1$ we have that the decay exponent is $\gamma = 2$ as shown in Figure 1.3.

If α is an even integer > 2 the same expansions lead to

$$\begin{aligned}\left[\mathrm{Li}_\alpha(\mathrm{e}^y) - \mathrm{Li}_\alpha(\mathrm{e}^{-y})\right]^2 =& \frac{4(H_{\alpha-1} - \ln y)^2}{(\alpha-1)!^2} y^{2\alpha-2} \\ &- \frac{\pi^2}{(\alpha-1)!^2} y^{2\alpha-2} \\ &- \frac{4\pi\mathrm{i}y^{2\alpha-2}}{(\alpha-1)!^2}(H_{\alpha-1} - \ln y) \\ &- \frac{4\pi\mathrm{i}\zeta(\alpha-1)}{(\alpha-1)!} y^\alpha + \dots\end{aligned} \tag{1.201}$$

thus, the long-range behavior is driven by the same term ($\sim y^\alpha$) as for α odd, while if $\alpha = 2$ we have

$$[\mathrm{Li}_2(\mathrm{e}^y) - \mathrm{Li}_2(\mathrm{e}^{-y})]^2 = y^2(4 - 4\ln y - \pi^2)^2 - 4\pi i y^2\left(1 - \ln y\right) + \ldots \tag{1.202}$$

so

$$\begin{aligned} I_{\mathscr{C}_0} + I_{\mathscr{C}_{2\pi}} &= -\frac{1}{\mathrm{sgn}\,(1+\mu)(1+\mu)^2}\int_0^\infty \mathrm{d}y\, y^2\left(1 - \ln y\right)\mathrm{e}^{-yR} \\ &= \frac{1 - 2\gamma - 2\ln R}{\mathrm{sgn}\,(1+\mu)(1+\mu)^2}\frac{1}{R^3} \end{aligned} \tag{1.203}$$

($\gamma = 0.57721566$ is the Euler-Mascheroni constant). This shows a logarithmic correction to the expected scaling R^{-3}.

2
Dynamics of entanglement entropy crossing a quantum phase transition

The understanding of a one-dimensional equilibrium system often relies on a combination of analytical techniques (field theory, integrability, renormalization group approach) giving, for instance, either the exact or the very-well approximated low-energy (ground-state) properties in terms of effective models described by a few relevant quantities.

Away from equilibrium, when in the system is injected a huge amount of energy (for example after a quench), all the excited states take part in the dynamics and fewer analytical methods are available for analyzing them (for a complete review of both the experimental and the theoretical aspects, see Ref. [101]).

As entanglement measures revealed themselves as a powerful tool to characterize the universality class of quantum phase transitions, in this Chapter we will analyze the dynamical behavior of a closed quantum system, when crossing a phase transition, by looking at the dynamics of the entanglement entropy [38, 102–104], by investigating its evolution for the Ising chain in a time-dependent transverse field $h(t)$ as function of the speed with which we change $h(t)$.

We will examine the adiabatic regime (low speeds), the sudden-quench situation (high speed) and the cases with intermediate speeds. Then we will see how these results are related to the Kibble-Zurek mechanism [40–43, 105], by looking both at the scaling of entanglement entropy and the Schmidt gap [106] in the entanglement spectrum.

2.1 The model

In this work, we are interested in the time evolution of entanglement measures for the Ising model in a time dependent transverse field $h(t)$ [32]:

$$H = -\frac{1}{2}\sum_{j=1}^{L}\left[\sigma_j^x\sigma_{j+1}^x + h(t)\sigma_j^z\right] \tag{2.1}$$

where σ^x and σ^z are Pauli matrices.

We let $h(t)$ change linearly in time, from h_i to h_f

$$h(t) = h_i + sgn(h_f - h_i)\frac{t}{\tau} \tag{2.2}$$

where τ is the time scale (the inverse of the velocity) of the ramping and $0 < t < t_f$, with $t_f = |h_f - h_i|\tau$. The dynamics of the model is also exactly accessible [34, 107], as we will recall below.

We will be interested in the evolution of the entanglement entropy and the entanglement spectrum that can be computed according to the method in Appendix 1.B.

Let us consider a chain containig L sites, divided into two equally-spaced subsystems A and B containing $\ell = L/2$ adjacent sites.

The reduced density matrix of A, ρ_A is obtained from the pure density matrix of the ground state $|GS(t)\rangle$ evolved in time by (2.1), by tracing out the degrees of freedom of B:

$$\rho_A(t) = \mathrm{Tr}_B\, |GS(t)\rangle \langle GS(t)| \tag{2.3}$$

We can define the entanglement Hamiltonian [108] $\mathscr{H}$ of $\rho_A(t)$ as $\rho_A(t) = \mathrm{e}^{-\mathscr{H}(t)}$ and its energy spectrum as the entanglement spectrum (ES). We will be also interested in the set $\{\zeta_n(t)\}$ of the eigenvalues of $\rho_A(t)$ from which it is possible to compute the von Neumann entropy

$$S_{L/2}(t) = -\mathrm{Tr}\,\rho_A(t)\log_2\rho_A(t) = -\sum_n \zeta_n(t)\log_2\zeta_n(t). \tag{2.4}$$

In the following sections, we will study the evolution of $S_{L/2}(t)$ during the ramping of $h(t)$ from the paramagnetic sector of the phase diagram ($h_i > 1$) to the ferromagnetic one ($h_f < 1$). This turns out to be also the setting for the Kibble-Zurek mechanism in the 1D quantum Ising model.

We choose a system of $L = 50$ (postponing the discussion of size-effects to Sec. 2.3), and and $h_i = 1.4$ to $h_f = 0.4$ for the ramping.

We show how to describe the dynamics of a state according to the Hamiltonian in Eq. 2.1. We follow the procedure of Ref. [109].

A Jordan-Wigner transformation (Appendix 1.A) can cast Hamiltonian (2.1) in a free fermionic model

$$H = -\frac{1}{2}\sum_{j=1}^{L}\left[\left(c_{j+1}^\dagger c_j + c_{j+1}c_j + h.c.\right) - 2h(t)c_j^\dagger c_j\right] - \frac{Lh(t)}{2} \tag{2.5}$$

The time evolution of the system in eq. (2.5) is described by the Heisenberg equation for the c operators:

$$\mathrm{i}\frac{\mathrm{d}}{\mathrm{d}t}c_j(t) = \left[c_j(t), H_j(t)\right] \tag{2.6}$$

which can be rewritten as:

$$\mathrm{i}\frac{\mathrm{d}}{\mathrm{d}t}c_j(t) = \sum_{k=1}^{L}\left[A_{jk}(t)c_k(t) + B_{jk}(t)c_k^\dagger(t)\right] \tag{2.7}$$

with

$$A_{jk}(t) = h(t)\delta_{jk} - \frac{1}{2}\left(\delta_{j,k+1} + \delta_{j+1,k} - \delta_{j1}\delta_{kL} - \delta_{jL}\delta_{k1}\right) \tag{2.8}$$

$$B_{jk}(t) = -\frac{1}{2}\left(\delta_{j+1,k} - \delta_{j,k+1} + \delta_{j1}\delta_{kL} - \delta_{jL}\delta_{k1}\right). \tag{2.9}$$

In order to solve such an equation, we make the following ansatz, known as time-dependent Bogolyubov transformation:

$$c_j(t) \equiv \sum_{m=0}^{L-1}\left[u_{jm}(t)b_m + v_{jm}^*(t)b_m^\dagger\right] \tag{2.10}$$

with the initial conditions $u_{jm}(0) = u_{jm}$ and $v_{jm}(0) = v_{jm}$ given by the initial Bogolyubov angles (1.127)

$$u_{jm} = \frac{\mathrm{e}^{\mathrm{i}k_m j}}{\sqrt{L}}\cos\theta_n = \frac{\mathrm{e}^{\mathrm{i}k_m j}}{\sqrt{L}}\sqrt{\frac{1}{2} + \frac{h(0)+\cos k_m}{2\lambda(k_m)}} \tag{2.11}$$

$$v_{jm} = \frac{\mathrm{e}^{\mathrm{i}k_m j}}{\sqrt{L}}\sin\theta_n = \frac{\mathrm{e}^{\mathrm{i}k_m j}}{\sqrt{L}}\sqrt{\frac{1}{2} - \frac{h(0)+\cos k_m}{2\lambda(k_m)}} \tag{2.12}$$

where $\lambda(k_m)$ is the dispersion relation (1.130) $\lambda(k_m) = \sqrt{(h(0)+\cos k_m)^2 + \sin^2 k_m}$.

By putting the ansatz of eq. (2.10) in the Heisenberg equation, we come to the set of linear coupled differential equations

$$\begin{aligned}\mathrm{i}\frac{\mathrm{d}}{\mathrm{d}t}u_{jm}(t) &= \sum_{k=1}^{L}\left[A_{jk}(t)u_{km}(t) + B_{jk}(t)v_{km}(t)\right]\\ -\mathrm{i}\frac{\mathrm{d}}{\mathrm{d}t}v_{jm}(t) &= \sum_{k=1}^{L}\left[B_{jk}(t)u_{km}(t) + A_{jk}(t)v_{km}(t)\right]\end{aligned} \tag{2.13}$$

that can be solved by standard techniques.

Once computed $c_j(t)$ one can construct the correlation matrices $\mathbb{C}_{ij} = \langle c_j^\dagger(t)c_i(t)\rangle$ and $\mathbb{F}_{ij} = \langle c_j^\dagger(t)c_i^\dagger(t)\rangle$ and compute the entanglement spectrum by following section 1.B.1.

Unless explicitly stated, we choose $L = 50$ (postponing the discussion of size-effects to Sec. 2.3), and show our results for a ramping from $h_i = 1.4$ to $h_f = 0.4$. We choose these values of the initial and final magnetic field in order to restrict the range of integration of the differential equations eq. (2.13).

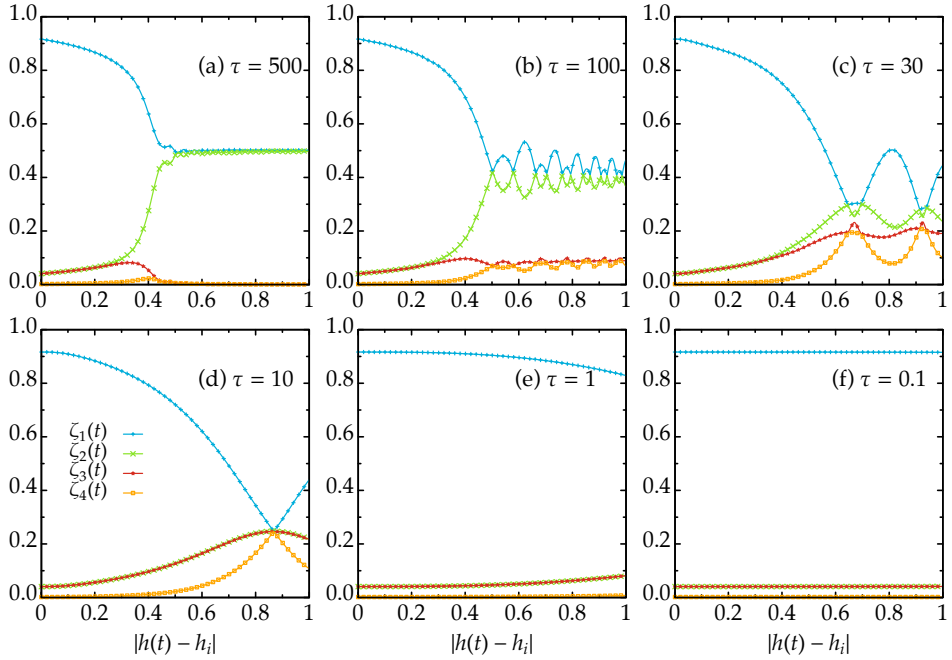

Figure 2.1: Dynamics of the first four eigenvalues of $\rho_A(t)$ for $L = 50$, $h_i = 1.4$ and $h_f = 0.4$. Different panels refer to different τ. In panels (d) , (e) and (f) the red and green lines overlay.

2.2 Dynamics of the entanglement

In this section we will study the dynamics of the entanglement spectrum and of the entanglement entropy in detail (Figs. 2.1 and 2.2).

Their evolution in time displays different behaviors depending on the values of τ. We can identify four regimes:

(i) adiabatic regime, $\tau \sim 500$;

(ii) slow regime $\tau \gtrsim 20$;

(iii) fast regime $1 \lesssim \tau \lesssim 20$;

(iv) sudden regime $\tau \lesssim 1$;

we will discuss in the following sections.

2.2.1 *Adiabatic and sudden regimes*

We begin by considering very large values of τ, i.e., a quasi-adiabatic quench, see for example the curve panel (a) of Fig. 2.1 and at $\tau = 500$ of Fig. 2.2.

We observe that during the evolution the entanglement entropy and the entanglement spectrum closely follow the static values, i.e. those obtained

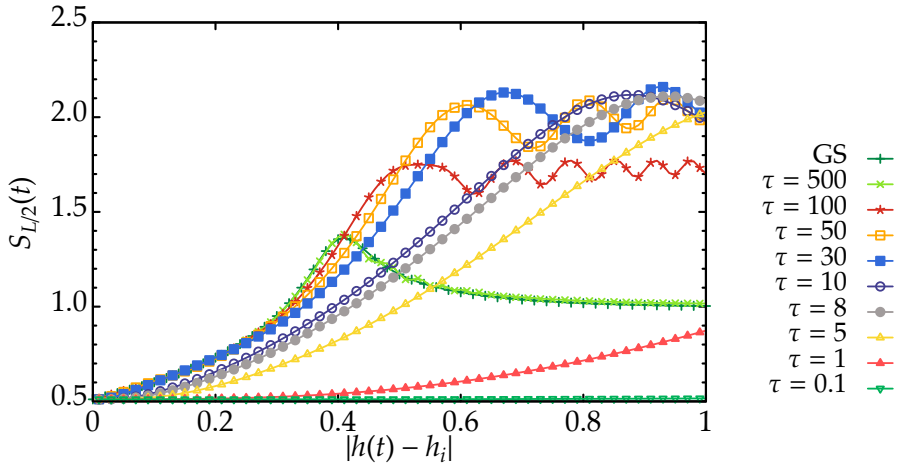

Figure 2.2: Dynamics of the entanglement entropy $S_{L/2}(t)$ for $L = 50$, $h_i = 1.4$, $h_f = 0.4$ for different values of τ.

from the ground state of the system at each value of $h(t)$, the only difference being represented by some small oscillations, that will be discussed in section 2.2.3.

This behavior is expected as the gap, because of the finite size of the system, remains non-zero for any finite L and the adiabatic theorem holds [110] provided τ is large enough.

We then consider the opposite regime, with very small values of τ, i.e., very fast quenches (curve with $\tau = 0.1$ in Fig. 2.2) and panel (f) of Fig. 2.1. The entanglement entropy and the entanglement spectrum do not evolve at all, as expected from the adiabatic theorem, independently on the size of the system.

2.2.2 *Fast sweeps*

We consider now rampings that are slower than sudden ones, but much faster than adiabatic ones; we call them fast sweeps, and, for our system sizes, they correspond to $1 \lesssim \tau \lesssim 20$. We consider the faster regime $\tau \sim 1$ and then the slower rampings $10 \lesssim \tau \lesssim 20$.

Starting from faster rampings (see curves with $\tau = 1$ and 5 in Figure 2.2), the entanglement entropy increases linearly in the region close to the phase transition: this behavior can be related to the results of Calabrese and Cardy [38] relative to a sudden quench to a conformal critical point where the entanglement entropy is predicted to grow linearly (see eq. (1.89)).

In our case, even if the ramping is not sudden, the picture of [38] can be also applied because, close to the critical point, the correlation length and the relaxation time are large, so the system behaves as critical for a finite interval of h.

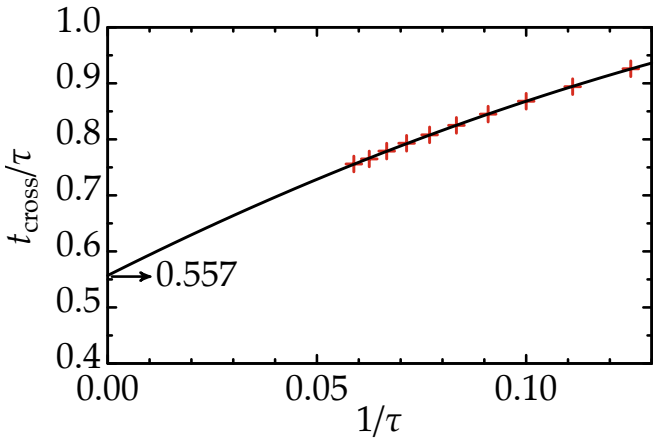

Figure 2.3: The plot shows the time at which the eigenvalues of the reduced density matrix cross as a function of $1/\tau$, for $8 < \tau < 17$. This time results to be always larger than the critical one, meaning that the oscillations start only after the system has reached the critical point. Red crosses: numerical data. Black line: fitting formula $a_0 + a_1/\tau + a_2/\tau^2$, giving $a_0 = 0.557$ (critical point: 0.4).

The behavior of the entanglement spectrum is of course related to the one of the entanglement entropy and it is shown in panel (e) of Figure 2.1.

In this regime of τ, the growth of the entanglement entropy can be ascribed to the decreasing of the first eigenvalue and to the increasing of the other three [111].

Remarkably, $\zeta_2(t)$ and $\zeta_3(t)$ are still degenerate. They indeed correspond, at $t = 0$, to the degenerate eigenstates $|1\rangle$ and $|L/2\rangle$ (see Appendix 2.A), and the time evolution does not break the degeneracy, at least for these values of τ.

The second regime is encountered by further increasing τ (see for example curves with $\tau = 8, 10$ and 30 in the main panel of Figure 2.2). In such cases, the entanglement entropy still presents a linear-growth region ending in an oscillatory region, in which the entanglement entropy alternates between maxima and minima, with variable frequency.

This behavior has already been observed in a thermodynamic-limit study of the dynamics of entanglement entropy [104], and has been ascribed to the fact that the system ends up, after passing the critical point, in a superposition of excited states of the instantaneous Hamiltonian.

We now investigate the behavior of the entanglement spectrum in this regime. As shown in panel (d) of Figure 2.1, the decreasing of $\zeta_1(t)$ and the growth of the remaining eigenvalues continues until they cross, all at the same point. The fourfold crossing, we observed, is actually a crossing between the first and the fourth eigenvalue, while the second and the third continue evolving parallel to each other.

Moreover, this crossing structure recurs also for later times in an almost periodic pattern.

The crossings correspond, as expected, to the maxima of entanglement entropy and this oscillatory behavior starts only after the system has crossed the critical point.

This fact is easily confirmed by plotting the crossing time t_{cross} as a function of τ: the result is shown in Figure 2.3: the data can be fitted by a power-law:

$$\frac{t_{\text{cross}}}{\tau} = a_0 + \frac{a_1}{\tau} + \frac{a_1}{\tau^2} \tag{2.14}$$

showing that, for $\tau \gg 1$, the crossing point is always greater than the critical one (the latter being equal to 0.4). (strictly speaking, we could not take the limit $\tau \to \infty$, since, for larger τ, the behavior of the system tends to become adiabatic; however, this extrapolation shows that the oscillations, also present for larger τ, always have the same nature; see Sec. 2.2.3).

We have also verified that the crossing time t_{cross} does not depend on the size of the system at fixed τ. This fact represents a further evidence of the fact that the physics, for these values of τ, coincides with the thermodynamic-limit one.

2.2.3 *Slow sweeps*

The last regime is observed for $\tau \gtrsim 20$. As Figure 2.1(c) shows, the second and the third eigenvalues begin to separate, making the crossing of $\zeta_1(t)$ and $\zeta_4(t)$ an avoided crossing. For larger values of τ, as shown in figure 2.1(b), this separation continues and the dynamical structure of the spectrum gets closer to the static one, i.e., the one of figure 2.1(a).

Remarkably, the crossings, occurring between the $\zeta_1(t)$ and $\zeta_2(t)$ and between $\zeta_3(t)$ and $\zeta_4(t)$, take place at the same times for the first and the second couple.

On the other hand, the entanglement entropy, as shown in the main panel of Figure 2.2 (curve with $\tau = 100$), at the beginning of the evolution is practically coincident with the static one, and at a certain point begins to grow and to oscillate around a value smaller than the ones of section 2.2.2 and decreasing as τ increases.

The behavior of the entanglement spectrum and the entanglement entropy can be ascribed to the approaching of the adiabatic regime. However, as already observed in section 2.2.1, the oscillation (now between the first and the second two eigenvalues) studied in section 2.2.2 survive as a sign of non-adiabaticity.

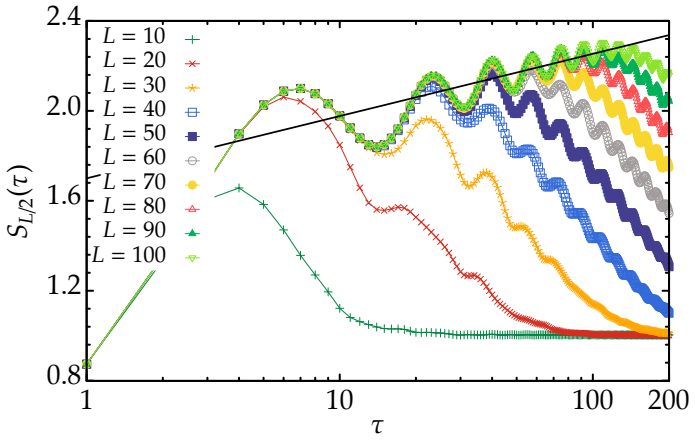

Figure 2.4: Entanglement entropy at the final instant of the evolution for $1 < \tau < 200$ at different system sizes ($10 \leq L \leq 100$, from top to bottom). The equation of the black line is const. + $(\log_2 \tau)/12$.

2.3 Kibble-Zurek physics

In this Section, we discuss the Kibble-Zurek scaling [40–43] of the entanglement entropy already considered and of the Schmidt gap [106, 112], i.e., the difference between the two largest eigenvalues in the entanglement spectrum. A discussion of this mechanism for the XY-model may be found in Refs. [105, 113–115].

In its original formulation, the Kibble-Zurek mechanism is able, on the basis of extremely simple approximations, to predict the scaling of the number of topological defects produced after the dynamical transition of a critical point.

The key assumption underlying the mechanism is that the evolution can be divided, for suitable ramping velocities, into three parts: a first adiabatic one, where the wave function of the system coincides with the ground state of $H(t)$; a second it impulsive, where the wave function of the system is practically frozen, due to the large relaxation time close to the critical point; a third adiabatic one, as the system is driven away from the critical point [105].

This division takes the name of adiabatic-impulse-adiabatic approximation [116, 117]. What plays a role in this kind of mechanism is the correlation length ξ at the times of passage between the different regimes, that can be seen to scale, for a linear quench of inverse velocity τ, as [42, 43]

$$\xi \approx \tau^{\frac{\nu}{1+z\nu}} \tag{2.15}$$

being ν and z the critical exponents of the crossed quantum critical point [118].

2.3.1 *Entanglement entropy*

Any quantity that is directly related to the correlation length ξ is suitable to a Kibble-Zurek analysis. In particular, close to a conformal critical point of conformal charge c, the entanglement entropy has been shown to scale as [31]:

$$S = \frac{c}{6} \log_2 \xi + \text{const.} \tag{2.16}$$

and therefore the entanglement entropy after the quench is easily seen to scale as [104]

$$S_{L/2}(\tau) = \frac{c\nu}{6(1+z\nu)} \log_2 \tau + \text{const.} \tag{2.17}$$

The prefactor of the logarithm would be $1/24$, since in the Ising case $\nu = z = 1$ and $c = 1/2$, but as the subsystem A has two boundaries we need to double the prefactor of the logarithm. So we expected the entropy to scale as [31, 102]

$$S_{L/2}(\tau) = \frac{1}{12} \log_2 \tau + \text{const.} \tag{2.18}$$

This clearly holds in the thermodynamic limit, where the gap is strictly closed at the critical point.

At finite size, we expect some deviations from the Kibble-Zurek behavior for large τ. We plot the results we obtain in Figure 2.4: as expected, we observe a progressive breakdown of the Kibble-Zurek prediction lowering L.

Moreover, it is evident that the logarithmic behavior expected from the Kibble-Zurek mechanism is superimposed to an oscillating behavior, as already observed in Ref. [104]: it is clearly a reflex of the oscillating structure of the entanglement entropy as a function of time, studied in Sec. 2.2.2 and 2.2.3.

Third, we observe that, for small values of τ, the curves at different sizes are practically coincident. This coincidence is lost for larger values of τ, depending on L: the velocities at which this coincidence is observed are the ones at which the physics is practically the one of the thermodynamic limit. For example, at $L = 50$, the physics is practically the thermodynamic limit one up to $\tau \approx 15$.

Finally, we note that, remarkably, the τ that correspond to the passage from the fast to the slow regime (the τ for which the crossing between the first and the fourth eigenvalue of the reduced density matrix begin to disappear), correspond to the breakdown of the Kibble-Zurek, or, equivalently, of the thermodynamic-limit physics.

This fact could be verified by a direct thermodynamic-limit investigation (as, e.g., in [104]), and it could represent, in principle, a very simple tool to check the equivalence between finite-size and thermodynamic-limit physics.

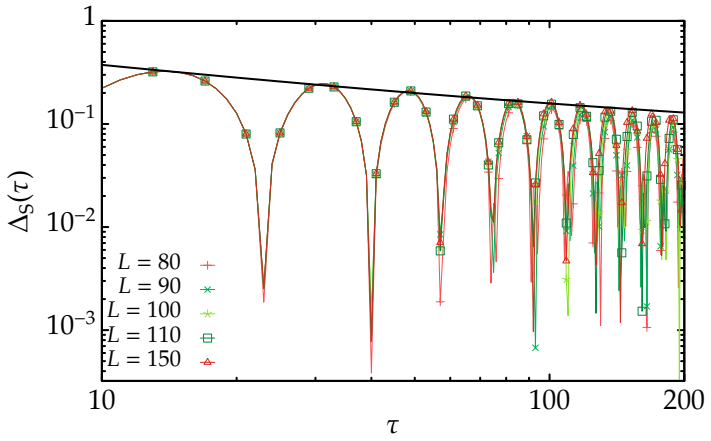

Figure 2.5: Schmidt gap at the final instant of the evolution for $10 < \tau < 200$ at different system sizes ($80 \leq L \leq 150$, from top to bottom). The equation of the black line is const. + $\tau^{-1/2}$.

2.3.2 *Schmidt gap*

As already mentioned above, the Schmidt gap Δ_S is defined as the difference between the two highest eigenvalues of the reduced density matrix. It has been very recently shown [106] to be related to the correlation length

$$\Delta_S \approx \xi^{-z} \tag{2.19}$$

and therefore its Kibble-Zurek scaling is

$$\Delta_S \approx \tau^{-\frac{z\nu}{1+z\nu}} = \tau^{-1/2} \tag{2.20}$$

Figure 2.5 shows the data for the scaling of the of the Schmidt gap at the end of the ramping as a function of τ with the function $\Delta_S = \tau^{-1/2} + \text{const}$ that surprisingly interpolates with extreme precision the maxima of $\Delta_S(\tau)$ numerically computed.

At fixed L, the shape of each curve shows also non-analyticities as a function of τ that are a consequence of the crossing of the eigenvalues of the reduced density matrix.

Thus, as for the entanglement entropy, we found also eq. (2.20) to be compatible with the numerical results.

2.4 Conclusions

In this Chapter we have examined the dynamical evolution of the quantum Ising chain in a time-dependent transverse magnetic field by looking at the evolution of the entanglement entropy and the entanglement spectrum, that, in recent years, have been used to investigate the physics of a closed quantum system crossing a phase transition.

We observed qualitatively different regimes: an adiabatic one (large τ) when the system evolves according the instantaneous ground state, a sudden quench (small τ) when the system is essentially frozen to its initial state and an intermediate one where entropy starts growing linear in time and then displays oscillations due to, among the others, some level crossing happening in the entanglement spectrum.

The entanglement spectrum can be used also to study both universal quantities (scaling exponents) and physical phenomena, such as the Kibble-Zurek mechanism, that may manifest during the evolution.

Appendices

2.A Initial structure of the entanglement spectrum

In this section we compute the reduces density matrix for the ground state of the Ising model (2.1) at $t = 0$ in the limit $h(0) = h \to \infty$. The ground state of the system is

$$|0\rangle = |\uparrow\rangle_1 |\uparrow\rangle_2 \cdots |\uparrow\rangle_L \tag{2.21}$$

where $|\uparrow\rangle_j$ and $|\downarrow\rangle_j$ are the eigenstates of σ_j^z.

This is not the exact ground state for $h \gg 1$, but, at first order in perturbation theory, it is easy to show that the latter is given by

$$|GS\rangle = \mathscr{N}\left[|0\rangle + \frac{1}{4h}\sum_{j=1}^{L}|j, j+1\rangle\right] \tag{2.22}$$

with

$$|j, j+1\rangle = |\uparrow\rangle_1 |\uparrow\rangle_2 \cdots |\downarrow\rangle_j |\downarrow\rangle_{j+1} \cdots |\uparrow\rangle_{L-1} |\uparrow\rangle_L \tag{2.23}$$

being the state where the spins at sites j and $j+1$ are flipped and $\mathscr{N} = \left(1 + \frac{L}{16h^2}\right)^{-\frac{1}{2}}$ is a normalization factor.

The zero-temperature density matrix of the system is given by $|GS\rangle\langle GS|$ and the reduced density matrix ρ_A of the half chain $A = \{1, \cdots, L/2\}$ takes the form

$$\rho_A = \begin{pmatrix} |0\rangle_A, & |2p\rangle_A, & |1\rangle_A, & |L/2\rangle_A \end{pmatrix} \mathbb{R}_A \begin{pmatrix} {}_A\langle 0| \\ {}_A\langle 2p| \\ {}_A\langle 1| \\ {}_A\langle L/2| \end{pmatrix} \tag{2.24}$$

with

$$|0\rangle_A = |\uparrow\rangle_1 |\uparrow\rangle_2 \cdots |\uparrow\rangle_{L/2} \tag{2.25}$$

$$|2p\rangle_A = \left(\frac{L}{2} - 1\right)^{-\frac{1}{2}} \sum_{j=1}^{\frac{L}{2}-1} |j, j+1\rangle \tag{2.26}$$

$$|1\rangle_A = |\downarrow\rangle_1 |\uparrow\rangle_2 \cdots |\uparrow\rangle_L \tag{2.27}$$

$$|L/2\rangle_A = |\uparrow\rangle_1 |\uparrow\rangle_2 \cdots |\uparrow\rangle_{L/2-1} |\downarrow\rangle_{L/2} \tag{2.28}$$

and

$$\mathbb{R}_A = \mathscr{N}^2 \begin{pmatrix} 1 + \frac{\frac{L}{2}-1}{16h^2} & \frac{\sqrt{\frac{L}{2}-1}}{4h} & 0 & 0 \\ \frac{\sqrt{\frac{L}{2}-1}}{4h} & \frac{\frac{L}{2}-1}{16h^2} & 0 & 0 \\ 0 & 0 & \frac{1}{16h^2} & 0 \\ 0 & 0 & 0 & \frac{1}{16h^2} \end{pmatrix} \tag{2.29}$$

$\mathbb{R}_A$ shows that $|1\rangle_A$ and $|L/2\rangle_A$ are degenerate eigenstates of ρ_A with eigenvalues

$$\zeta_{2,3} = \frac{1}{2\ell + 16h^2} \tag{2.30}$$

with $\ell = L/2$.

Diagonalizing the remaining block gives the others two eigenvalues

$$\zeta_{1,4} = \frac{(\ell - 1)/2 + 4h^2 \pm 2\sqrt{h^2\left(\ell + 4h^2 - 1\right)}}{\ell + 8h^2}. \tag{2.31}$$

For large enough h, the two eigenstates related to $\zeta_{1,4}$ are superpositions of $|0\rangle_A$ and $|2p\rangle_A$, one in which the paramagnetic state $|0\rangle_A$ dominates and the other in which $|2p\rangle_A$ dominates. A numerical analysis shows also that $\zeta_1 < \zeta_2 = \zeta_3 < \zeta_4$, for sufficiently high h.

3
Résumé en Français

Les récents progrès expérimentaux dans le piégeage et dans la manipulation de gaz atomiques et moléculaires ultra-froids [1–3] ont permis d'explorer et de simuler beaucoup de phénomènes qui arrivent dans des systèmes a N corps à l'équilibre ou hors de l'équilibre (transitions de phase quantiques [4], phases fortement corrélées [5], évolution quantique [12], propagation des corrélations et des quasi-particules [19]).

Les réseaux optiques sont l'exemple clef de systèmes où les atomes peuvent être piégés et les interactions entre eux peuvent être contrôlées avec une extrême versatilité.

Il est possible aussi de modifier le rayon de ces interactions en employant, par exemple, des ions piégés [19, 26, 27] qui ont été utilisés avec succès pour créer des potentiels inversement proportionnels à la distance r comme $1/r^{\alpha}$ où α peut varier approximativement de 0 à 3, en permettant la simulation de beaucoup de modèles [du champ moyen ($\alpha = 0$) à l'interaction dipôle-dipôle ($\alpha = 3$)].

A cause des précédents résultats expérimentaux dans la première partie de la thèse, nous étudierons quel est le rôle joué par un terme à long rayon d'action ajouté à une Hamiltonienne locale, en caractérisant le diagramme de phase par des quantités non locales (comme, par exemple, l'entropie d'intrication et le comportement de corrélations).

Le modèle qui en résulte est une généralisation de la chaîne de Kitaev [29] et il décrit un système fermionique avec un pairing p-wave à long rayon qui tombe avec la distance telle qu'une puissance avec exposant α.

L'Hamiltonienne de Kitaev a été étudiée en [29] comme modèle pour l'ordre quantique topologique. Une phase topologique dans une dimension est caractérisée par la présence de deux ou plus d'états fondamentaux dégénérés qui paraissent sans la brisure d'une symètrie locale de l'Hamiltonienne et par la localisation d'edge modes, identifiés comme des modes de Majorana, lesquels, peuvent être théoriquement employés comme qubits.

Le modèle étudié est encore quadratique et, donc, exactement résoluble. En en employant l'intégrabilité nous avons démontré l'existence de deux régimes massifs, l'un où les fonctions de corrélation tombent exponentiellement à de courtes distances et comme puissance à de longues distances, l'autre où elles tombent à puissance seulement.

Dans la seconde région, en outre, l'entropie d'intrication d'un sous-système

diverge logarithmiquement. Les deux résultats sont inattendus pour des phases massives d'Hamiltoniennes locales (où l'entropie d'intrication devient constante [31] et les corrélations tombent exponentiellement [30]) et ils sont caractéristiques de systèmes avec des interactions à long rayon qui montrent leurs effets dans le comportement de quantités non locales comme les corrélations et l'entropie d'intrication.

Si l'on considère la limite $\alpha \to \infty$ le modèle devient celui d'Ising, amplement étudié [32–34] car il est exactement résoluble et, au même temps, car il est à même d'expliquer des phénomènes pas banals. On peut le considérer aussi comme un paradigme pour les transitions de phase quantiques [35] entre une phase paramagnétique et antiferromagnétique séparées par un point critique qui appartient à la classe d'universalité du modèle d'Ising décrit par une théorie conforme [36, 37].

Après avoir introduit le terme à long rayon, en variant α, ce point devient une ligne critique qui n'est plus décrite par une théorie conforme pour des α suffisamment petits. On a prouvé ça en calculant l'évolution temporelle de l'entropie d'entanglement après un quench.

On a trouvé [38] que dans un modèle invariant sous les transformations conformes, l'entropie croît linéairement dans le temps. On peut comprendre ça en pensant qu'après un quench des couples de quasi-particules sont créés dans un point du système. Ces quasi-particules sont entangled et se déplacent avec une vitesse de groupe non nulle. Si l'on coupe le système en deux parités (A et B) le nombre de particules créées en A qui arrivent en B croît linéairement avec le temps (du moment que la vitesse de groupe est constante) et également, l'intrication entre les deux parties change linéairement dans le temps.

L'évolution temporelle de l'entropie dans la chaîne avec le pairing a long rayon est, au contraire, logarithmique lorsque $\alpha < 1$. Le même résultat a été trouvé dans le modèle d'Ising [39] et, dans la description à quasi-particules, il peut être expliqué par l'existence d'une vitesse divergente. Nous avons trouvé, en effet, le point exacte dans le diagramme de phase où la vitesse des excitations diverge et nous avons montré que pour cette valeur-là l'évolution de l'entropie d'intrication n'est plus linéaire.

Par rapport au problème de la dynamique dans des systèmes quantiques, la seconde partie de la thèse étudie l'évolution de l'entropie d'intrication et de l'intrication spectrum lorsque le système traverse une transition de phase avec de différentes vitesses.

Comme exemple, on peut dire que nous avons arrêté notre attention sur le modèle d'Ising avec un champ magnétique qui dépend linéairement du temps:

$$H_{\text{Ising}} = \sum_i \left[\sigma_i^x \sigma_{i+1}^x - h(t)\sigma_i^z\right] \tag{3.1}$$

où $\sigma_i^{(x,z)}$ sont matrices de Pauli.

Le champ magnétique change comme $h(t) = h_i + \frac{t}{\tau}$ où τ est l'inverse de la vitesse avec laquelle le système est approché du point de transition et h_i peut se trouver soit dans la phase paramagnétique que dans l'antiferromagnétique.

Nous avons calculé l'évolution temporelle de l'entropie d'intrication et nous avons trouvé de différents régimes qui dépendent de la vitesse de transition: un régime adiabatique (de basses vitesses, de grands τ) lorsque le système évolue selon son état fondamental instantané; un sudden quench (de hautes vitesses, de bas τ) lorsque le système est essentiellement congelé dans son état initial; un régime intermédiaire où l'entropie croît linéairement et, ensuite, elle montre des oscillations du moment que, après avoir passé le point critique, le système se trouve dans une superposition des états excités de l'Hamiltonienne instantanée.

Nous avons discuté aussi du mécanisme de Kibble-Zurek [40–43] qui donne une estimation de la densité de défauts topologiques produits après la transition lorsque la longueur de corrélation ξ diverge. Ces défauts sont produits sur des distances plus petites que ξ qui satisfait $\xi \sim \tau^{\nu/(\nu z+1)}$ où ν et z sont les exposants critiques de la transition.

Du moment que l'entropie S sature à une valeur $S \sim \log \xi$, nous avons montré, enfin, que pour l'argument de Kibble-Zurek, l'entropie dépend de l'inverse de la vitesse τ comme $S \sim \log \tau$.

4
Riassunto in Italiano

I recenti progressi sperimentali nell'intrappolamento e la manipolazione di gas atomici e molecolari ultrafreddi [1–3] hanno offerto la possibilità di esplorare e simulare un'ampia classe di fenomeni che avvengono in sistemi a molti corpi fuori e all'equilibrio (transizioni di fase quantistiche [4], fasi della materia fortemente correlate [5], evoluzione quantistica [12], propagazione dinamica dei correlatori e quasiparticelle [19]).

I reticoli ottici sono l'esempio chiave di sistemi in cui gli atomi posso essere intrappolati e le interazioni tra di essi posso essere controllate con estrema versatilità.

È diventato inoltre possibile modificare anche il raggio di tali interazioni, impiegando, ad esempio, ioni intrappolati [19, 26, 27] che sono stati utilizzati con successo per creare potenziali che decadono con la distanza r come $1/r^{\alpha}$ dove α può variare, approssimativamente, da 0 a 3, permettendo la simulazione di una grande classe di modelli [dal campo medio ($\alpha = 0$) all'interazione dipolo-dipolo ($\alpha = 3$)].

Motivati da questi risultati sperimentali, nella prima parte della tesi, studieremo qual è il ruolo giocato da un termine a lungo raggio aggiunto ad una Hamiltoniana locale, caratterizzando il diagramma di fase tramite quantità non locali (quali ad esempio l'entropia di entanglement e il decadimento dei correlatori).

Il modello che ne risulta è una generalizzazione della catena di Kitaev [29] che descrive un sistema fermionico con un pairing p-wave a lungo raggio che decade con la distanza come una potenza con esponente α.

L'Hamiltoniana di Kitaev con solo termini on site e a primi vicini è stata studiata come modello per l'ordine topologico. Una fase topologica in una dimensione è caratterizzata dalla presenza di due o più stati fondamentali degeneri che appaiono senza la rottura di una simmetria locale della Hamiltoniana e dalla localizzazione di modi di edge, identificati come modi di Majorana, che, in principio posso essere utilizzati, nelle applicazioni di informatica quansti, come qubits.

Il modello a lungo raggio studiato, contenendo essenzialmente dei termini di pairing, è ancora quadratico e quindi esattamente risolubile.

Sfruttandone l'integrabilità, abbiamo dimostrato l'esistenza di due regimi massivi, uno in cui le funzioni di correlazione decadono esponenzialmente a corte distanze e a potenza a lunghe, l'altro in cui decadono pura-

mente a potenza.

Nella seconda regione, inoltre, l'entropia di entanglement di un sotto sistema diverge logaritmicamente. Entrambi questi risultati sono inaspettati per fasi massive di Hamiltoniane locali (dove l'entropia di entanglement diventa costante [31] e i correlatori decadono esponenzialmente [30]) e sono caratteristici di sistemi con forti interazioni a lungo raggio che mostrano i propri effetti nel comportamento di quantità non locali come le correlazioni e l'entropia di entanglement.

Considerando il limite $\alpha \to \infty$ il modello diventa quello di Ising, ampiamente studiato sia perché esattamente risolubile e, allo stesso tempo, perché è in grado di spiegare fenomeni non banali. Può essere, inoltre, considerato come un paradigma per le transitions de phase quantiques tra una fase paramagnetica e ordinata separate da un punto critico appartenente alla classe di universalità del modello d'Ising descritto da une teoria conforme.

Una volta introdotto il termine a lungo raggio, tale punto, variando α diventa una linea critica che, per α sufficientemente piccoli non è più descritto da une théorie conforme. Questo è stato anche provato calcolando l'evoluzione temporale dell'entropia di entanglement dopo un quench.

In un modello invariante conforme, è stato provato che l'entropia cresce linearmente nel tempo. Ciò può esser compreso pensando che, dopo un quench, coppie di quasi-particelle vengono create in un dato punto del sistema. Queste quasi-particelle sono entangled e si muovono con velocità di gruppo non nulla.

Se ora si divide il sistema in due parti (A e B) il numero di particelle create in A che arrivano in B cresce linearmente con il tempo (dato che la velocità di gruppo è costante) e, allo stesso modo, l'entanglement tra le due parti varia linearmente nel tempo.

L'evoluzione temporale dell'entropia nella catena con il pairing a lungo raggio è, invece, logaritmica quando $\alpha < 1$. Lo stesso avviene nel modello di Ising e ciò può esser spiegato, nella descrizione a quasi particelle, perché esiste una velocità divergente. Abbiamo, infatti, trovato il punto esatto nel diagramma di fase per cui la velocità delle eccitazione diverge e abbiamo mostrato che per quel valore l'evoluzione dell'entropia di entanglement non è più lineare.

In relazione al problema della dinamica in sistemi quantistici chiusi, la seconda parte della tesi affronta lo studio dell'evoluzione dell'entropia di entanglement e dell'entanglement spectrum quando il sistema attraversa una transizione di fase con diverse velocità.

Come esempio, ci siamo soffermati sul modello di Ising con un campo magnetico linearmente dipendente dal tempo:

$$H_{\text{Ising}} = \sum_i \left[\sigma_i^x \sigma_{i+1}^x - h(t)\sigma_i^z\right] \tag{4.1}$$

dove $\sigma_i^{(x,z)}$ sono matrici di Pauli.

Il campo magnetico varia come $h(t) = h_i + \frac{t}{\tau}$, dove τ è l'inverso della velocità con cui il sistema viene avvicinato al punto di transizione e h_i può essere sia nella fase paramagnetica $h_i > 1$ o in quella ordinata $h_i < 1$.

Abbiamo calcolato l'evoluzione temporale dell'entropia di entanglement di mezza catena e abbiamo trovato diversi regimi che dipendono dalla velocità della transizione: un regime adiabatico (basse velocità, grandi τ) quando il sistema evolve secondo il suo stato fondamentale istantaneo; un sudden quench (alte velocità, bassi τ) quando il sistema è essenzialmente congelato nel suo stato iniziale; un regime intermedio in cui l'entropia cresce linearmente e, in seguito, mostra delle oscillazioni dato che il sistema, dopo aver passato il punto critico, si trova in una sovrapposizione di stati eccitati della Hamiltoniana istantanea.

Abbiamo inoltre discusso il meccanismo di Kibble-Zurek che predice il numero di difetti topologici prodotti dopo la transizione nella fase cosiddetta impulsiva, quando la lunghezza di correlazione ξ comincia a divergere. Tali difetti vengono prodotti su distanze minori di ξ che soddisfa $\xi \sim \tau^{\nu/(\nu z+1)}$ dove ν and z sono gli esponenti critici della transizione.

Dato che l'entropia S satura a un valore $\sim \log \xi$ [31], si è mostrato, infine, che per l'argomento di Kibble-Zurek, l'entropia dipende dall'inverse della velocità τ come $S \sim \log \tau$.

Ringrazio i miei relatori, prof.ssa Elisa Ercolessi e prof. Guido Pupillo non solo per l'opportunità che ho avuto di lavorare con loro e per le dritte in Fisica che mi hanno dato, ma anche per i consigli di vita che ho ricevuto. Ringrazio Luca L. e Luca T. che hanno avuto un ruolo fondamentale nella stesura di questa tesi. Senza di loro non sarebbe mai venuta fuori. Grazie!

Un grazie va anche a Piero e Francesco ed Edoardo, che hanno reso più accettabili le ore passate in quella gattabuia a Bologna e a Strasburgo (e non solo).

Ringrazio il prof. Fabio Ortolani, Marcello Dalmonte, Marion Moliner, Rogelio Diaz-Mendez, Enrique Rico, Adriano Angelone e Zhe-Xuan Gong e Alexey Gorshkov per avermi ospitato al JQI.

Ringrazio Fabio che ha cercato sempre di farmi diventare un buon fisico, ma con scarsi risultati (non per colpa sua). Senza di lui molte serate a Strasburgo non sarebbero per niente passate.

Bibliography

[1] I. Bloch, J. Dalibard, and W. Zwerger, Many-body physics with ultracold gases, Rev. Mod. Phys. **80**, 885 (2008).

[2] I. Bloch, J. Dalibard, and S. Nascimbene, Quantum simulations with ultracold quantum gases, Nat. Phys. **8**, 267 (2012).

[3] R. Blatt and C. F. Roos, Quantum simulations with trapped ions, Nat Phys **8**, 277 (2012).

[4] M. Greiner, O. Mandel, T. Esslinger, T. W. Hansch, and I. Bloch, Quantum phase transition from a superfluid to a Mott insulator in a gas of ultracold atoms, Nature **415**, 39 (2002).

[5] T. Kinoshita, T. Wenger, and D. S. Weiss, Observation of a One-Dimensional Tonks-Girardeau Gas, Science **305**, 1125 (2004).

[6] E. Haller, R. Hart, M. J. Mark, J. G. Danzl, L. Reichsollner, M. Gustavsson, M. Dalmonte, G. Pupillo, and H.-C. Nagerl, Pinning quantum phase transition for a Luttinger liquid of strongly interacting bosons, Nature **466**, 597 (2010).

[7] B. Paredes, A. Widera, V. Murg, O. Mandel, S. Folling, I. Cirac, G. V. Shlyapnikov, T. W. Hansch, and I. Bloch, Tonks-Girardeau gas of ultracold atoms in an optical lattice, Nature **429**, 277 (2004).

[8] B. DeMarco and D. S. Jin, Onset of Fermi Degeneracy in a Trapped Atomic Gas, Science **285**, 1703 (1999).

[9] C. A. Regal, M. Greiner, and D. S. Jin, Observation of Resonance Condensation of Fermionic Atom Pairs, Phys. Rev. Lett. **92**, 040403 (2004).

[10] C. Chin, M. Bartenstein, A. Altmeyer, S. Riedl, S. Jochim, J. H. Denschlag, and R. Grimm, Observation of the Pairing Gap in a Strongly Interacting Fermi Gas, Science **305**, 1128 (2004).

[11] M. Greiner, O. Mandel, T. W. Hansch, and I. Bloch, Collapse and revival of the matter wave field of a Bose-Einstein condensate, Nature **419**, 51 (2002).

[12] T. Kinoshita, T. Wenger, and D. S. Weiss, A quantum Newton's cradle, Nature **440**, 900 (2006).

[13] L. E. Sadler, J. M. Higbie, S. R. Leslie, M. Vengalattore, and D. M. Stamper-Kurn, Spontaneous symmetry breaking in a quenched ferromagnetic spinor Bose-Einstein condensate, Nature **443**, 312 (2006).

[14] D. Chen, M. White, C. Borries, and B. DeMarco, Quantum Quench of an Atomic Mott Insulator, Phys. Rev. Lett. **106**, 235304 (2011).

[15] M. Cheneau, P. Barmettler, D. Poletti, M. Endres, P. Schausz, T. Fukuhara, C. Gross, I. Bloch, C. Kollath, and S. Kuhr, Light-cone-like spreading of correlations in a quantum many-body system, Nature **481**, 484 (2012).

[16] U. Schneider, L. Hackermuller, J. P. Ronzheimer, S. Will, S. Braun, T. Best, I. Bloch, E. Demler, S. Mandt, D. Rasch, and A. Rosch, Fermionic transport and out-of-equilibrium dynamics in a homogeneous Hubbard model with ultracold atoms, Nat Phys **8**, 213 (2012).

[17] S. Trotzky, Y.-A. Chen, A. Flesch, I. P. McCulloch, U. Schollwock, J. Eisert, and I. Bloch, Probing the relaxation towards equilibrium in an isolated strongly correlated one-dimensional Bose gas, Nat Phys **8**, 325 (2012).

[18] J. P. Ronzheimer, M. Schreiber, S. Braun, S. S. Hodgman, S. Langer, I. P. McCulloch, F. Heidrich-Meisner, I. Bloch, and U. Schneider, Expansion Dynamics of Interacting Bosons in Homogeneous Lattices in One and Two Dimensions, Phys. Rev. Lett. **110**, 205301 (2013).

[19] P. Richerme, Z.-X. Gong, A. Lee, C. Senko, J. Smith, M. Foss-Feig, S. Michalakis, A. V. Gorshkov, and C. Monroe, Non-local propagation of correlations in quantum systems with long-range interactions, Nature **511**, 198 (2014).

[20] I. Bloch, Ultracold quantum gases in optical lattices, Nat Phys **1**, 23 (2005).

[21] U. Fano, Effects of Configuration Interaction on Intensities and Phase Shifts, Phys. Rev. **124**, 1866 (1961).

[22] H. P. Büchler, E. Demler, M. Lukin, A. Micheli, N. Prokof'ev, G. Pupillo, and P. Zoller, Strongly Correlated 2D Quantum Phases with Cold Polar Molecules: Controlling the Shape of the Interaction Potential, Phys. Rev. Lett. **98**, 060404 (2007).

[23] A. Micheli, G. Pupillo, H. P. Büchler, and P. Zoller, Cold polar molecules in two-dimensional traps: Tailoring interactions with external fields for novel quantum phases, Phys. Rev. A **76**, 043604 (2007).

[24] T. Lahaye, C. Menotti, L. Santos, M. Lewenstein, and T. Pfau, The physics of dipolar bosonic quantum gases, Reports on Progress in Physics **72**, 126401 (2009).

[25] G. Pupillo, A. Micheli, Büchler, and P. Zoller, Condensed Matter Physics with Cold Polar Molecules, in *Cold Molecules: Theory, Experiment, Applications*, edited by R. Krems, B. Friedrich, and S. W. C. (CRC Press, 2009).

[26] J. W. Britton, B. C. Sawyer, A. C. Keith, C. C. J. Wang, J. K. Freericks, H. Uys, M. J. Biercuk, and J. J. Bollinger, Engineered two-dimensional Ising interactions in a trapped-ion quantum simulator with hundreds of spins, Nature **484**, 489 (2012).

[27] R. Islam, C. Senko, W. C. Campbell, S. Korenblit, J. Smith, A. Lee, E. E. Edwards, C.-C. J. Wang, J. K. Freericks, and C. Monroe, Emergence and Frustration of Magnetism with Variable-Range Interactions in a Quantum Simulator, Science **340**, 583 (2013).

[28] P. Jurcevic, B. P. Lanyon, P. Hauke, C. Hempel, P. Zoller, R. Blatt, and C. F. Roos, Quasiparticle engineering and entanglement propagation in a quantum many-body system, Nature **511**, 202 (2014).

[29] A. Y. Kitaev, Unpaired Majorana fermions in quantum wires, Physics-Uspekhi **44**, 131 (2001).

[30] M. Hastings and T. Koma, Spectral Gap and Exponential Decay of Correlations, Comm. Math. Phys. **265**, 781 (2006).

[31] P. Calabrese and J. Cardy, Entanglement entropy and quantum field theory, J. Stat. Mech. **2004**, P06002 (2004).

[32] E. Lieb, T. Schultz, and D. Mattis, Two soluble models of an antiferromagnetic chain, Annals of Physics **16**, 407 (1961).

[33] E. Barouch, B. M. McCoy, and M. Dresden, Statistical Mechanics of the XY Model. I, Phys. Rev. A **2**, 1075 (1970).

[34] E. Barouch and B. M. McCoy, Statistical Mechanics of the XY Model. II. Spin-Correlation Functions, Phys. Rev. A **3**, 786 (1971).

[35] S. Sachdev, *Quantum phase transitions*, 2nd ed. (Cambridge University Press, Cambridge, England, 2011).

[36] G. Mussardo, *Statistical Field Theory, An Introduction to Exactly Solved Models in Statistical Physics* (Oxford University Press, New York, 2010).

[37] M. Henkel, *Conformal Invariance and Critical Phenomena* (Springer, New York, 1999).

[38] P. Calabrese and J. Cardy, Evolution of entanglement entropy in one-dimensional systems, J. Stat. Mech. **2005**, P04010 (2005).

[39] J. Schachenmayer, B. P. Lanyon, C. F. Roos, and A. J. Daley, Entanglement Growth in Quench Dynamics with Variable Range Interactions, Phys. Rev. X **3**, 031015 (2013).

[40] T. W. B. Kibble, Topology of cosmic domains and strings, Journal of Physics A: Mathematical and General **9**, 1387 (1976).

[41] T. Kibble, Some implications of a cosmological phase transition, Physics Reports **67**, 183 (1980).

[42] W. H. Zurek, Cosmological experiments in superfluid helium?, Nature **317**, 505 (1985).

[43] W. Zurek, Cosmological experiments in condensed matter systems, Physics Reports **276**, 177 (1996).

[44] P. Jordan and E. Wigner, Über das Paulische Äquivalenzverbot, Zeitschrift für Physik **47**, 631 (1928).

[45] A. Belavin, A. Polyakov, and A. Zamolodchikov, Infinite conformal symmetry in two-dimensional quantum field theory, Nuclear Physics B **241**, 333 (1984).

[46] F. W. J. Olver, D. W. Lozier, R. F. Boisvert, and C. W. Clark, *NIST Handbook of Mathematical Functions* (Cambridge University Press, Cambridge, England, 2010).

[47] M. J. Ablowitz and A. S. Fokas, *Complex Variables Introduction and Applications*, 2nd ed. (Cambridge University Press, New York, 2003).

[48] T. Koffel, M. Lewenstein, and L. Tagliacozzo, Entanglement Entropy for the Long-Range Ising Chain in a Transverse Field, Phys. Rev. Lett. **109**, 267203 (2012).

[49] G. Vidal, J. I. Latorre, E. Rico, and A. Kitaev, Entanglement in Quantum Critical Phenomena, Phys. Rev. Lett. **90**, 227902 (2003).

[50] J. I. Latorre, E. Rico, and G. Vidal, Ground State Entanglement in Quantum Spin Chains, Quantum Info. Comput. **4**, 48 (2004).

[51] A. Anfossi, C. D. E. Boschi, A. Montorsi, and F. Ortolani, Single-site entanglement at the superconductor-insulator transition in the Hirsch model, Phys. Rev. B **73**, 085113 (2006).

[52] L. Amico, R. Fazio, A. Osterloh, and V. Vedral, Entanglement in many-body systems, Rev. Mod. Phys. **80**, 517 (2008).

[53] P. Calabrese, J. Cardy, and B. Doyon, Entanglement entropy in extended quantum systems, Journal of Physics A: Mathematical and Theoretical **42**, 500301 (2009).

[54] M. Dalmonte, E. Ercolessi, and L. Taddia, Estimating quasi-long-range order via Rényi entropies, Physical Review B **84**, 085110 (2011).

[55] S. Nishimoto, Tomonaga-Luttinger-liquid criticality: Numerical entanglement entropy approach, Phys. Rev. B **84**, 195108 (2011).

[56] M. Dalmonte, E. Ercolessi, and L. Taddia, Critical properties and Rényi entropies of the spin-3/2 XXZ chain, Physical Review B **85**, 165112 (2012).

[57] X. Deng, R. Citro, E. Orignac, A. Minguzzi, and L. Santos, Bosonization and entanglement spectrum for one-dimensional polar bosons on disordered lattices, New Journal of Physics **15**, 045023 (2013).

[58] Y. Chen, P. Zanardi, Z. D. Wang, and F. C. Zhang, Sublattice entanglement and quantum phase transitions in antiferromagnetic spin chains, New Journal of Physics **8**, 97 (2006).

[59] J. I. Cirac and F. Verstraete, Renormalization and tensor product states in spin chains and lattices, Journal of Physics A: Mathematical and Theoretical **42**, 504004 (2009).

[60] J. Eisert, M. Cramer, and M. B. Plenio, *Colloquium*: Area laws for the entanglement entropy, Rev. Mod. Phys. **82**, 277 (2010).

[61] C. Holzhey, F. Larsen, and F. Wilczek, Geometric and renormalized entropy in conformal field theory, Nuclear Physics B **424**, 443 (1994).

[62] S. R. White, Density matrix formulation for quantum renormalization groups, Phys. Rev. Lett. **69**, 2863 (1992).

[63] S. R. White, Density-matrix algorithms for quantum renormalization groups, Phys. Rev. B **48**, 10345 (1993).

[64] U. Schollwöck, The density-matrix renormalization group, Rev. Mod. Phys. **77**, 259 (2005).

[65] M. B. Hastings, Lieb-Schultz-Mattis in higher dimensions, Phys. Rev. B **69**, 104431 (2004).

[66] P. di Francesco, P. Mathieu, and D. Senechal, *Conformal Field Theory* (Springer, 1997).

[67] P. Ginsparg, Curiosities at $c = 1$, Nuclear Physics B **295**, 153 (1988).

[68] P. Ginsparg, Applied conformal field theory, in *Fields, Strings and Critical Phenomena, Les Houches Lecture Notes, Session XLIX*, edited by E. Brézin and J. Zinn-Justin (1988).

[69] T. Giamarchi, *Quantum Physics in One Dimensions*, International Series of Monographs on Physics, Vol. 121 (Clarendon, Oxford, 2004).

[70] P. Calabrese and J. Cardy, Entanglement and correlation functions following a local quench: a conformal field theory approach, Journal of Statistical Mechanics: Theory and Experiment **2007**, P10004 (2007).

[71] V. Eisler and I. Peschel, Evolution of entanglement after a local quench, Journal of Statistical Mechanics: Theory and Experiment **2007**, P06005 (2007).

[72] M. Fagotti and P. Calabrese, Evolution of entanglement entropy following a quantum quench: Analytic results for the XY chain in a transverse magnetic field, Phys. Rev. A **78**, 010306 (2008).

[73] J.-M. Stéphan and J. Dubail, Local quantum quenches in critical one-dimensional systems: entanglement, the Loschmidt echo, and light-cone effects, Journal of Statistical Mechanics: Theory and Experiment **2011**, P08019 (2011).

[74] M. Collura, S. Sotiriadis, and P. Calabrese, Quench dynamics of a Tonks–Girardeau gas released from a harmonic trap, Journal of Statistical Mechanics: Theory and Experiment **2013**, P09025 (2013).

[75] M. G. Nezhadhaghighi and M. A. Rajabpour, Entanglement dynamics in short- and long-range harmonic oscillators, Phys. Rev. B **90**, 205438 (2014).

[76] G. D. Chiara, S. Montangero, P. Calabrese, and R. Fazio, Entanglement entropy dynamics of Heisenberg chains, Journal of Statistical Mechanics: Theory and Experiment **2006**, P03001 (2006).

[77] P. Hauke and L. Tagliacozzo, Spread of Correlations in Long-Range Interacting Quantum Systems, Phys. Rev. Lett. **111**, 207202 (2013).

[78] V. Alba and F. Heidrich-Meisner, Entanglement spreading after a geometric quench in quantum spin chains, Phys. Rev. B **90**, 075144 (2014).

[79] G. Torlai, L. Tagliacozzo, and G. D. Chiara, Dynamics of the entanglement spectrum in spin chains, Journal of Statistical Mechanics: Theory and Experiment **2014**, P06001 (2014).

[80] A. J. Daley, C. Kollath, U. Schollwöck, and G. Vidal, Time-dependent density-matrix renormalization-group using adaptive effective Hilbert spaces, Journal of Statistical Mechanics: Theory and Experiment **2004**, P04005 (2004).

[81] S. R. White and A. E. Feiguin, Real-Time Evolution Using the Density Matrix Renormalization Group, Phys. Rev. Lett. **93**, 076401 (2004).

[82] G. Vidal, Efficient Simulation of One-Dimensional Quantum Many-Body Systems, Phys. Rev. Lett. **93**, 040502 (2004).

[83] A. E. Feiguin and S. R. White, Time-step targeting methods for real-time dynamics using the density matrix renormalization group, Phys. Rev. B **72**, 020404 (2005).

[84] E. H. Lieb and D. W. Robinson, The finite group velocity of quantum spin systems, Communications in Mathematical Physics **28**, 251 (1972).

[85] M. Foss-Feig, Z.-X. Gong, C. W. Clark, and A. V. Gorshkov, Nearly-linear light cones in long-range interacting quantum systems, ArXiv e-prints (2014), arXiv:1410.3466 [quant-ph] .

[86] J. Eisert, M. van den Worm, S. R. Manmana, and M. Kastner, Breakdown of Quasilocality in Long-Range Quantum Lattice Models, Phys. Rev. Lett. **111**, 260401 (2013).

[87] M. A. Rajabpour and S. Sotiriadis, Quantum quench in long-range field theories, ArXiv e-prints (2014), arXiv:1409.6558 [cond-mat.str-el] .

[88] E. Majorana, Teoria simmetrica dell'elettrone e del positrone, Il Nuovo Cimento **14**, 171 (1937).

[89] P. Fendley, Parafermionic edge zero modes in Z n -invariant spin chains, Journal of Statistical Mechanics: Theory and Experiment **2012**, P11020 (2012).

[90] J. L. van Hemmen and G. Vertogen, A note on Fermi lattice systems with bilinear hamiltonians: The XY model once morse, Physica A: Statistical Mechanics and its Applications **81**, 391 (1975).

[91] J. van Hemmen, A note on the diagonalization of quadratic boson and fermion hamiltonians, Zeitschrift für Physik B Condensed Matter **38**, 271 (1980).

[92] J. P. Blaizot and G. Ripka, *Quantum Theory of Finite Systems* (MIT Press, 1986).

[93] F. Pientka, L. I. Glazman, and F. von Oppen, Phys. Rev. B **88**, 155420 (2013).

[94] A. Its, F. Mezzadri, and M. Mo, Entanglement Entropy in Quantum Spin Chains with Finite Range Interaction, Communications in Mathematical Physics **284**, 117 (2008).

[95] M. Abramowitz and I. A. Stegun, *Handbook of Mathematical Functions* (Dover, 1964).

[96] I. Peschel and T. T. Truong, Corner transfer matrices and conformal invariance, Z. Phys. B **69**, 385 (1987).

[97] T. T. Truong and I. I. Peschel, Diagonalisation of finite-size corner transfer matrices and related spin chains, Z. Phys. B **75**, 119 (1989).

[98] I. Peschel, M. Kaulke, and O. Legeza, Density-matrix spectra for integrable models, Ann. Phys. (Leipzig) **8**, 153 (1999).

[99] I. Peschel, Calculation of reduced density matrices from correlation functions, J. Phys. A **36**, L205 (2003).

[100] I. Peschel, Special Review: Entanglement in Solvable Many-Particle Models, Brazilian Journal of Physics **42**, 267 (2012).

[101] A. Polkovnikov, K. Sengupta, A. Silva, and M. Vengalattore, *Colloquium*: Nonequilibrium dynamics of closed interacting quantum systems, Rev. Mod. Phys. **83**, 863 (2011).

[102] L. Cincio, J. Dziarmaga, M. M. Rams, and W. H. Zurek, Entropy of entanglement and correlations induced by a quench: Dynamics of a quantum phase transition in the quantum Ising model, Phys. Rev. A **75**, 052321 (2007).

[103] T. Caneva, R. Fazio, and G. E. Santoro, Adiabatic quantum dynamics of the Lipkin-Meshkov-Glick model, Phys. Rev. B **78**, 104426 (2008).

[104] F. Pollmann, S. Mukerjee, A. G. Green, and J. E. Moore, Dynamics after a sweep through a quantum critical point, Phys. Rev. E **81**, 020101 (2010).

[105] W. H. Zurek, U. Dorner, and P. Zoller, Dynamics of a Quantum Phase Transition, Phys. Rev. Lett. **95**, 105701 (2005).

[106] G. De Chiara, L. Lepori, M. Lewenstein, and A. Sanpera, Entanglement Spectrum, Critical Exponents, and Order Parameters in Quantum Spin Chains, Phys. Rev. Lett. **109**, 237208 (2012).

[107] B. M. McCoy, E. Barouch, and D. B. Abraham, Statistical Mechanics of the XY Model. IV. Time-Dependent Spin-Correlation Functions, Phys. Rev. A **4**, 2331 (1971).

[108] H. Li and F. D. M. Haldane, Entanglement Spectrum as a Generalization of Entanglement Entropy: Identification of Topological Order in Non-Abelian Fractional Quantum Hall Effect States, Phys. Rev. Lett. **101**, 010504 (2008).

[109] T. Caneva, R. Fazio, and G. E. Santoro, Adiabatic quantum dynamics of a random Ising chain across its quantum critical point, Phys. Rev. B **76**, 144427 (2007).

[110] A. Messiah, *Quantum Mechanics* (Dover Publications, Mineola, 1999).

[111] M. A. Nielsen and I. L. Chuang, *Quantum Computation and Quantum Information* (Cambridge University Press, Cambridge, 2000).

[112] L. Lepori, G. De Chiara, and A. Sanpera, Scaling of the entanglement spectrum near quantum phase transitions, Phys. Rev. B **87**, 235107 (2013).

[113] J. Dziarmaga, Dynamics of a Quantum Phase Transition: Exact Solution of the Quantum Ising Model, Phys. Rev. Lett. **95**, 245701 (2005).

[114] A. Polkovnikov, Universal adiabatic dynamics in the vicinity of a quantum critical point, Phys. Rev. B **72**, 161201 (2005).

[115] V. Mukherjee, U. Divakaran, A. Dutta, and D. Sen, Quenching dynamics of a quantum XY spin-$\frac{1}{2}$ chain in a transverse field, Phys. Rev. B **76**, 174303 (2007).

[116] B. Damski, The Simplest Quantum Model Supporting the Kibble-Zurek Mechanism of Topological Defect Production: Landau-Zener Transitions from a New Perspective, Phys. Rev. Lett. **95**, 035701 (2005).

[117] B. Damski and W. H. Zurek, Adiabatic-impulse approximation for avoided level crossings: From phase-transition dynamics to Landau-Zener evolutions and back again, Phys. Rev. A **73**, 063405 (2006).

[118] G. Morandi, F. Napoli, and E. Ercolessi, *Statistical Mechanics: An Intermediate Course*, 2nd ed. (World Scientific, Singapore, 2001).